[redacted]

SEMI-ANNUAL TECHNICAL REPORT

SYNTHESIS OF COMPOUND SEMICONDUCTING MATERIALS AND DEVICE APPLICATIONS

July 1, 1971 - December 31, 1971

Grant No. DAHC15 71-G-9

The views and conclusions contained in this document are those of the authors and should not be interpreted as necessarily representing the official policies, either expressed or implied, of the Advanced Research Projects Agency or the U. S. Government.

[redacted]

CMR-72-2

CENTER FOR MATERIALS RESEARCH

STANFORD UNIVERSITY • STANFORD, CALIFORNIA

Semi-Annual Technical Report

July 1, 1971 - December 31, 1971

Sponsored by
Advanced Research Projects Agency
ARPA Order No. 1644

Program Code Number: POD10

Contractor: Stanford University

Grant No. DAHC15 71-G-9

Principal Investigator: D. A. Stevenson
Phone: (415) 321-2300, Ext. 4251

Co-Investigators:
R. H. Bube, Ext. 2535
R. S. Feigelson, Ext. 4007
G. S. Kino, Ext. 72289
B. L. Mattes, Ext. 2695
W. D. Nix, Ext. 4259
R. K. Route, Ext. 2695
W. A. Tiller, Ext. 2301

Effective Date of Grant: July 1, 1971

Grant Expiration Date: June 30, 1972

Amount of Grant $184,140

Grant Title: Synthesis of Compound Semiconducting Materials and Device Applications

Center for Materials Research
Stanford University
Stanford, California 94305
(415) 321-2300, Ext. 4118

CMR 72-2

TABLE OF CONTENTS

I. INTRODUCTION

The present program concerns the synthesis of compound semiconducting materials, with particular emphasis on their use in planar microwave devices. The program consists of three major sections: thin film epitaxial growth of III-V compounds; device design, fabrication and evaluation; and fundamental studies of crystal syntehsis and properties.

The devices of primary interest are of the planar microwave and acoustical type, employing thin films of GaAs as the active layer. The choice of GaAs was made based on its unique properties: exceptionally high carrier mobility, a moderately large band gap, the Gunn effect and piezoelectric response. These planar devices require high quality active layers of GaAs, with particularly strict requirements on film thickness, surface smoothness, and carrier density and mobility in the film. The layers are grown in the present study by liquid phase epitaxial techniques.

In the period covered by this report there have been three major accomplishments relating to materials synthesis and device fabrication: reproducible growth has been achieved for GaAs films with superior properties for microwave device applications; very thin layers (0.5 - 1.5 μ) of GaAs with optically smooth surfaces have been grown by liquid phase epitaxial techniques; and successful contacts have been made to the GaAs using an Ag-In-Ge alloy. Also during this period, significant progress has been made on the fundamental studies of crystal synthesis and properties of compound semiconductors. The topics include: observations of precipitation effects in GaAs by transmission electron microscopy; measurement of electrical property changes in GaAs induced by changes in dislocation density; and a theoretical analysis of the GaAs/liquid gallium interface. A description of progress in these developments is given below.

II. EPITAXIAL CRYSTAL GROWTH

R. S. Feigelson, B. L. Mattes, R. K. Route, and J. Yen

A. PROGRAM OBJECTIVE

The principal objective of the epitaxial crystal growth program is the preparation of high quality, uniform and reproducible epitaxial layers of GaAs for the device applications program. The device program requires layers (not obtainable commercially) that have carrier densities in the low 10^{14} cm^{-3} range, 300/77°K mobilities above 7000/50,000 cm^2/V-sec, thicknesses in the 1-30μm range, and optically smooth surfaces. All of these requirements are currently being achieved by liquid phase epitaxial techniques.

In order to meet this objective considerable effort has been devoted to the development of new methods of growth, the study of variables that influence growth, techniques to prepare and handle materials involved in growth, and methods to evaluate the growth and its properties. In addition the epitaxial crystal growth program is coordinated with the materials studies and device applications programs to prepare materials with specific properties and dimensions and to interact on problems of mutual concern.

The present objective of this program is to develop reliable ohmic contacts for epitaxial layers that have carrier densities in the 10^{14} cm^{-3} range. There is also a continued effort to improve the quality of the GaAs layers in anticipation of more stringent device requirements.

The future objectives of the epitaxial crystal growth program will be: (1) to meet the device application and materials study program requirements for III-V materials with specific properties; (2) to continue the development and evaluation of ohmic contacts on GaAs epitaxial layers; (3) to continue the analysis of the liquid phase growth process, in

particular nucleation; and (4) to develop new growth techniques for new devices.

B. PROGRESS

1. Achievements

High quality GaAs epitaxial layers, that meet the critical property requirements for the device application program, have been reproducibly grown by the liquid phase epitaxial method. The epitaxial crystal growth achievements during the past 6 months that led to this objective are (1) improvements in the purity of the growth system and materials--to yield low 10^{14} cm^{-3} carrier density material with 300/77°K mobilities of 8000/60,000 cm^2/V-sec; and (2) refinements in the temperature gradient cell--to yield layers with uniformity in thickness from .5 to 30μm and with optically smooth surfaces. These achievements demonstrate the success and potential of the liquid phase epitaxial method for the growth of high quality layers that in the past were only achieved by the vapor phase epitaxial method. During this 6 month period over 100 GaAs layers were grown, Table II-1. The majority of the layers were grown as part of the study of growth variables involved with the liquid phase epitaxial process. With the control of these variables reproducible high quality layers are now being grown.

The detailed study of the parameters involved in the growth process has shown that the initial stages of nucleation on the substrate determine the uniformity and quality of the layer. Because of this it appears that nucleation and growth are controlled by surface activation processes and are not diffusion limited.

The growth studies, results and future objectives will be discussed in the remainder of this chapter.

2. Preparation and Growth Methods

The growth processes and preparation techniques have been described in the previous Semi-Annual Technical Report[1] and Final Report.[2] The most significant change(s) that led to the improved purity of the layers appears to be related to one or all of the following: (1) new Ga solvent; (2) new GaAs source material; and (3) a new pyrolytic graphite boat. Each of the changes were introduced in the above order. It was found that low to mid 10^{14} cm^{-3} carrier density material was not obtained until the new pyrolytic boat was used. With the use of the new pyrolytic graphite boat, one could observe additional improvement in the quality of the material due to the new Ga solvent and the new GaAs source material. Besides the possibility of the new boat being purer, an essential difference between the boats was the procedure by which they were cleaned. Previously the old boats were fired in vacuum in an r.f. furnace at 1400 to 1500°C. The new boat, however, was fired in situ in hydrogen at 850°C for 24 hours. The improved results from this process suggest that perhaps the vacuum-r.f. system was contaminated.

Further refinements have also been made in the substrate polishing and preparation procedures as well as bake out procedures for the quartz reactor tube and Ga solvent.

Two other areas of development are underway: (1) the use of arsine to provide a source of As to saturate the Ga solvent, and to increase the partial pressure of As for the purpose of reducing As evaporation from the substrate; and (2) the use of a temperature gradient cell to deposit n^+ layers for reliable ohmic contacts to low 10^{14} cm^{-3}, n-type, carrier density material. These developments are based on results that were obtained from the growth studies, to be discussed next.

3. Growth Studies

It has been established that a temperature gradient normal to the liquid-solid interface stabilizes the layer surface and the uniformity in thickness of the layer. A large temperature gradient tends to eliminate terraces altogether. Temperature gradients have been measured directly in the melt and across the substrate during growth using thermocouple probes. The largest temperature gradients used in the temperature gradient cell are about 10°C/cm. It has also been observed that a high rate of cooling has the same effect as a large temperature gradient. Both of these parameters and their influence on growth are graphically shown in Figures II-1a and b. When thermal fluctuations, $\pm \Delta T$, are superimposed on the melting temperature, T_m, the uncertainty in the position of the interface is less when the temperature gradient, ∇T, is large. When the rate of cooling, dT/dt, is higher than the fluctuation rate, $\Delta T/P$, the freezing and melting at the interface is reduced to a smaller spatial range, Figure II-1b. Since the spacing between terraces and the growth velocity are very small, the terraces cannot be accounted for on the basis of constitutional supercooling or diffusion limited growth. To show this, consider the distance that As will diffuse in a Ga solution in 1 sec. From the diffusion equation $x \sim \sqrt{Dt}/2$, where the diffusion coefficient, D, for As in a Ga solution is 5×10^{-5} cm^2/sec and the maximum growth velocity, V, for GaAs is $\sim 10^{-6}$ cm/sec,[3] it is readily apparent that diffusion of the As occurs at $10^{-5}/10^{-12}$ times faster than the growth velocity.

Recently it was demonstrated that the terrace spacing is directly related to the number and spacing of nuclei on the substrate at the initial stages of growth. Figures II-2a and b show the initial hillocks that grew

from the heterogeneous nucleation on the surface and the final layer with terraces, respectively. This sequence of events was accomplished by tilting part of the As-saturated Ga melt off of a portion of the substrate and then allowing the remainder of the growth to go to completion. Note the correlation between spacing, form, orientation and delineation in the two regions on the same substrate. The direction of the terraces appears to be influenced by a slight transverse temperature gradient.

The shape of the hillocks during initial stages of nucleation depends on the orientation of the substrate. The (111)A and B substrates generally yield triangular or hexagonal hillocks while the (100) substrates yield square or rectangular hillocks. Both heterogeneous as well as homogeneous nucleation takes place on the substrate surface and in the Ga melt, respectively, during growth. If nucleation cannot take place on the substrate, due to impurities or another type of defect on the surface, a uniform epitaxial layer will not form. Instead, platelets form by homogeneous nucleation in the melt and the platelets close to the substrate become weakly attached to the substrate. Figure II-3 shows this effect on a (100) substrate that had a stain on the surface. Figures II-4a, b and c show a similar effect on a (111)B substrate where two variations of this type of defect are observed. Figure II-4b shows a hexagonal hillock attached to the surface of a layer. Figure II-4c shows a hexagonal depression in the layer that perhaps formed as a platelet formed above the layer in the melt. These defects are commonly observed when the As-saturated Ga melt becomes supersaturated. This occurs when the substrate temperature is well below the melt temperature at the time the melt is rolled onto the substrate. By equalizing the temperatures, this effect is reduced.

The saturation temperature appears to affect both the nucleation for the (100) and (111)A orientations, and the purity of the layer. This may be

related to the volatization of impurities, such as oxides. In general, higher quality layers are obtained for saturation temperatures above 700°C. For temperatures below this, temperature gradients greater than 10°C/cm must be imposed on (100) substrates to achieve a uniform layer without severe hillock formations. This is believed to be due to a lack of nucleation sites on the substrate and homogeneous nucleation in the melt.

Another type of defect has been frequently observed, as shown in Figure II-5a. This figure shows an extreme example. The defect is Ga inclusions in the layer, generally next to the substrate. This defect was traced to the evaporation of As from the surface of the GaAs substrate, leaving Ga behind, prior to growth. Figures II-5b, c and d show the different forms the Ga takes on (111)B, (111)A and (100) substrates, respectively. On the (111)B substrate surface, Figure II-5b, the Ga does not wet the surface hence the Ga is in the form of spheres. It was also observed that hydrogen flowing over the surface will blow these spheres along and leave a "track" behind. In some instances, these "tracks" are trenches in the substrate and in other cases they are layers or plateaus. The average amount of Ga left behind on the substrate is the same for all orientations, however the size and density varies for each orientation. Typically the Ga spheres on the (111)B substrate are 1 to 3μm in diameter. Some of these spheres also grow at the expense of others and may reach 20 μm in diameter. The large ones grossly affect the epitaxial layer, as shown in Figure II-5a. The residual Ga does not appear to dissolve into the Ga melt during growth, probably due to a crust of impurities on the residual Ga that comes from the heavily doped substrate. When the density of these defects is large, the carrier mobilities are abnormally low and the carrier density is high. The amount of evaporation can be reduced significantly by reducing the

time the substrate is exposed to elevated temperatures prior to growth, and/or by increasing the As partial pressure by introducing arsine into the system. The latter is most promising because of the practical requirement of heating the substrate during saturation.

Schottky barrier and van der Pauw measurements are routinely made on the layers to determine their carrier type, density, uniformity and mobility. Figures II-6a and b show typical carrier density profiles obtained on semi-insulating and n^+ substrates, respectively. It should be noted that with the use of the temperature gradient cell there is no insulating barrier between the epitaxial layer and the n^+ substrate.

Electron microprobe, emission spectrographic and photoluminescence techniques have been used in an attempt to identify impurities in the layers. Auger and mass spectrographic measurements are also contemplated in order to obtain more positive identifications of the impurities. Infrared microscopy is being used to identify inclusions and other defects in the layers and the substrates. Optical and electron microscopy are being used to study surface morphologies and layer thicknesses.

4. Growth Results

The liquid phase epitaxial method has yielded the high quality GaAs layers required for the device application program. The liquid phase methods developed have produced over 200 GaAs layers on semi-insulating and n^+ GaAs substrates. Table II-1 lists the layers and their properties that were grown over the past 6 months. Thirty of these layers met the high quality and uniformity required for device applications--carrier densities in the 10^{14} cm^{-3} range, mobilities above 7000 cm^2/V-sec, thicknesses in the 1-30μm range, and optically smooth surfaces. Because optically smooth 1μm layers are now obtainable by liquid phase epitaxial processes,

it is not now deemed essential to develop a vapor phase system.

Typical features of the growths obtained with and without a temperature gradient are shown in Figures II-7 and 8, respectively. Without a temperature gradient it is difficult to maintain uniformity in thickness over all the substrate. In small regions, however, the uniformity is quite good, Figures II-7b and c. Figures II-8a and b show a very uniform layer that is about 1μm thick. The terraces are extremely fine and are only found around small Ga inclusions on the substrate.

5. Ohmic Contact Studies

Because of the electrical contact problems encountered with low carrier density layers, the epitaxial crystal growth program is now devoting part of its time and techniques to solving this problem. From an extensive survey of the literature and the present "state of the art", n^+ contacts on 10^{14} cm^{-3} carrier density n-type layers appears to be the most reasonable solution. This type of contact is feasible with the present liquid phase epitaxial techniques. Alloy contacts, such as Au-Ge and Ag-In-Ge, are also under consideration for layers with carrier densities in and above the 10^{14} cm^{-3} range.

C. PROPOSED FUTURE WORK

The future objectives of the epitaxial crystal growth program will be to (1) maintain the present capability for preparing material for new device requirements; (2) evaluate and develop electrical contacts on high purity material for device applications; (3) study and analyze growth variables in the liquid phase epitaxial process; and (4) develop new growth techniques for III-V materials that may generate new devices and new concepts for their design.

The basic responsibility of the epitaxial crystal growth program is to provide materials that will meet specific property and dimensional requirements for the device program. Therefore the growth program must maintain a flexible capability to meet new requirements, which may include other III-V materials and their alloys. The facilities and technology for this capability has been established for GaAs but it may be extended to certain other III-V materials and their ternary solid solutions. The preparation of other materials may require the development of new growth methods, substrate preparation techniques and more detailed analyses of the growth conditions. For the majority of the device requirements, however, GaAs will be the primary material.

A study of the electrical contact problem will be initiated and will include a thorough evaluation of present techniques for low carrier density material as well as a study of new contacting procedures. New contacting procedures will be directed towards liquid phase grown n^+ contacts on n-type layers. The horizontal temperature gradient process will provide a unique method to deposit thin, uniform n^+ contacts on n-type layers without forming insulating layers at their interface. These features are necessary in order to perform precise photomasking-etching procedures, and to minimize contact resistance between the contact and active layer. Certain alloy contacts, such as Au-Ge and Ag-In-Ge, will also be useful for some applications. It is proposed to study their deposition and electrical contact to the layer by investigating the surface states on the layer, their wettability to the layer, and their diffusion into the layer. The scanning electron microscope in the current scan mode will be used as a very sensitive means to study the uniformity and performance of the contacts.

A continued effort will be made to study the variables that control growth in the liquid phase epitaxial process. Since the surface morphology

is determined by (1) the temperature at the start of growth, (2) the temperature gradients, (3) the rate of cooling, and (4) the substrate preparation, it appears that the morphology is related to the initial stages of nucleation. There is not only heterogeneous nucleation (growth on the substrate) but homogeneous nucleation (growth in the solvent) as well. The latter may be important in hillock formation that frequently occurs under certain conditions. If the process of nucleation is understood, more efficient techniques for epitaxial growth could be pursued to tailor growths for special device requirements. There will also be a continued effort to analyze the impurities in the layers to achieve higher mobilities and lower carrier densities. It is essential to know the impurities and their source if high quality GaAs is to be produced to meet device requirements. Low frequency noise measurements will be used to evaluate the suitability of the material for device applications.

Detailed studies of growth phenomena involved in liquid phase epitaxial processes has led to our ability to prepare high quality GaAs layers. Use of the present techniques and modification of growth variables will extend our capability of controlling the growth of layers and perhaps even allow the growth of GaAs layers on piezoelectric substrates. These types of developments will generate material for new devices and new designs for previous devices. The growth of tapered layers may help the performance of traveling wave devices by matching for losses incurred in the wave. Regional growth by masking techniques or hillock growth may give better isolation between devices or portions of a device on the same substrate. Growth of a GaAs layer on a piezoelectric substrate may give stronger coupling of acoustic or piezoelectric modes to the layer or vice versa. GaAs is a weak piezoelectric material compared to the oxide piezoelectrics or CdS.

The close contact maintained between the growth program and the device program has led and will continue to lead to the best means of supplying materials to meet specific properties and dimensions for device applications.

REFERENCES

1. Semi-Annual Technical Report, "Synthesis of Compound Semiconducting Materials and Device Applications", AD-718 878, ARPA Contract No. DAHC 15-70-G-12, Stanford University, July 1, 1970 - December 31, 1970.

2. Final Report, "Synthesis of Compound Semiconducting Materials and Device Applications", AD-727 803, ARPA Contract No. DAHC 15-70-G-12, Stanford University, July 1, 1970 - June 30, 1971.

3. J. A. Donahue, H. T. Minden, J. Crystal Growth 7, 221 (1970).

TABLE II-1

GaAs EPITAXIAL LAYER PROPERTIES

Growth No.*	Substrate Orientation†	Mobility RT/LN $cm^2/V\text{-}sec$	Carrier Density cm^{-3}	Thickness μm	Surface Morphology‡
139	(111)B	4,700/14,000	2×10^{16}	15	MT
140	(111)B	4,700/13,000	2×10^{16}	15	MT
141	(100)	Substrate Melt Back			
142	(100)	5,800/32,000	5×10^{15}	25	MT + GI
143	(100)	4,500/16,000	1×10^{16}	15	CT + GI
144	(111)B	5,600/25,000	5×10^{15}	21	MT
145	(111)B	5,700/44,000	9×10^{14}	23	CT
146	(111)B	6,200/46,000	4×10^{14}	15	MT
147	(111)B			15	MT
148	(111)B				MT + GI
149	(111)B				MT
150	(111)B	4,600/30,000	1×10^{15}	15	MT + GI
151	(111)B	5,500/31,000	4×10^{15}	15	FT + GI
152	(111)B	Surface Evaporation Study			
153	(111)B	Surface Evaporation Study			
154	(111)B	Surface Evaporation Study			

TABLE II-1 (cont.)

GaAs EPITAXIAL LAYER PROPERTIES

Growth No.*	Substrate Orientation†	Mobility RT/LN $cm^2/V\text{-}sec$	Carrier Density cm^{-3}	Thickness μm	Surface Morphology‡
155	(111)B	Substrate Melt Back			
156	(100)	Surface Evaporation Study			
157	(100)				FT
158	(111)A	Surface Evaporation Study			
159	(100)			15	FT + H
160	(111)A	4,700/30,000	4×10^{15}	27	FT
161	(100)	4,300/15,000			FT + GI
162	(100)	4,000/8,100	2×10^{16}	19	FT
163	(100)	5,400/26,000	7×10^{15}	21	ET
164	(111)B (LD)	5,200/23,000	8×10^{15}	20	ET
165	(111)B (LD)	4,400/31,000	2×10^{15}	24	ET
166	(111)B (LD)	4,500/16,000	1×10^{16}	22	ET
167	(111)B	4,200/15,000	7×10^{15}	30	FT
168	(111)B	5,500/17,000	2×10^{15}	15	FT
169	(111)B (LD)	2,600/7,400	5×10^{15}	20	ET + GI
170	(111)B (LD)	3,900/17,000	1×10^{16}	24	

TABLE II-1 (cont.)

GaAs EPITAXIAL LAYER PROPERTIES

Growth No.*	Substrate Orientation†	Mobility RT/LN $cm^2/V\text{-}sec$	Carrier Density cm^{-3}	Thickness μm	Surface Morphology‡
171	(100)			25	H
172	(100)			25	H
173	(100)	4,400/15,000	2×10^{16}	15	MT + GI
174	(111)B (LD)	3,900/32,000	6×10^{15}	25	ET
175	(100)				H
176	(111)B	4,600/12,000	3×10^{16}	14	MT
177	(100)	Surface Evaporation Study			
178 TG	(100)	5,200/21,000	1×10^{16}	13	FT + GI
179 TG	(100)	4,200/18,000	2×10^{16}	18	NT
180	(100)			20	H
181 TG	(111)A	6,300/8,800	4×10^{16}	10	ET
182 TG	(111)B (LD)	2,700/4,400	8×10^{15}	26	ET
183	(111)B (LD)	6,000/35,000	3×10^{15}	57	ET
184 TG	(100)	6,900/33,000	5×10^{15}	19	ET
185	(100)	4,800/12,000	3×10^{16}	16	FT + GI
186	(100)	3,800/8,400	2×10^{16}	14	MT + GI

TABLE II-1 (cont.)

GaAs EPITAXIAL LAYER PROPERTIES

Growth No.*	Substrate Orientation†	Mobility RT/LN $cm^2/V\text{-}sec$	Carrier Density cm^{-3}	Thickness μm	Surface Morphology‡
187 TG	(100)	2,300/3,700	6×10^{16}	6	MT + H + GI
188	(100)	3,300/3,600	1×10^{17}	8	FT + GI
189 TG	(100)	1,500/			H
190	(100)	1,500/	3×10^{16}	12	CT + H
191	(100)	3,900/6,700	3×10^{16}	9	MT + GI
192 TG	(100)	Substrate Melt Back			
193	(100)	3,300/6,600	3×10^{16}	17	MT + GI
194	(100)	3,100/13,000	2×10^{16}	13	CT
195 TG	(100)	5,600/16,000	1×10^{16}	20	ET + GI
196 TG	(100)	6,000/16,000	1×10^{16}	17	ET
197 TG	(100)	5,100/15,000	2×10^{16}	16	NT
198	(100)	5,800/21,000	7×10^{15}	30	ET
199 TG	(100)	5,600/17,000	8×10^{15}	20	NT
200	(100)	6,000/49,000	1×10^{15}	26	FT
201	(100)	5,900/28,000	3×10^{15}	47	FT
202 TG	(100)	5,400/25,000	3×10^{15}	26	ET

TABLE II-1 (Cont.)

GaAs EPITAXIAL LAYER PROPERTIES

Growth No.*	Substrate Orientation†	Mobility RT/LN $cm^2/V\text{-}sec$	Carrier Density cm^{-3}	Thickness μm	Surface Morphology‡
203 TG	(100)	5,500/30,000	1×10^{15}	20	MT + GI
204	(100)	4,600/13,000	2×10^{16}	25	MT
205	(111)B			25	ET
206 TG	(111)B	5,500/16,000	7×10^{15}	20	NT
207	(111)B	5,400/14,000	2×10^{16}	25	CT
208 TG	(111)B	3,600/7,100	4×10^{16}	6	NT
209	(111)B	5,800/24,000	1×10^{15}	25	MT
210	(111)B (LD)	5,800/32,000	3×10^{15}	9	ET
211 TG	(111)B	3,100/4,500	9×10^{16}	3	NT
212	(111)B	5,500/31,000	2×10^{15}	10	MT
213 TG	(111)B	6,400/23,000	3×10^{15}	3	NT
214	(111)B			25	FT
215 TG	(111)B	5,300/14,000	7×10^{15}	3	NT
216 TG	(111)B	4,900/8,900	6×10^{16}	2	NT
217	(111)B	7,100/22,000	9×10^{15}	18	CT
218	(111)B	7,000/34,000	2×10^{15}	18	ET

TABLE II-1 (Cont.)

GaAs EPITAXIAL LAYER PROPERTIES

Growth No.*	Substrate Orientation†	Mobility RT/LN $cm^2/V\text{-}sec$	Carrier Density cm^{-3}	Thickness μm	Surface Morphology‡
219	(111)B	8,000/53,000	8×10^{14}	22	ET
220	(111)B	7,800/59,000	5×10^{14}	12	ET
221 TG	(111)B	4,100/16,000	8×10^{15}	1	NT
222	(111)B	6,600/35,000	1×10^{15}	2-9	ET
223	(111)B	5,800/37,000	1×10^{14}	18	ET + H + GI
224 TG	(111)B n^+		2×10^{15}	3	NT
225	(111)B	6,400/26,000	7×10^{15}	22	ET
226	(111)B	6,500/59,000	5×10^{14}	18	ET + GI
227	(100)	8,200/50,000	5×10^{14}	10	FT
228	(100)	8,000/54,000	1×10^{15}	15	ET
229 TG	(111)B	3,100/	3×10^{17}	3	NT
230	(111)B	7,200/51,000	6×10^{14}	5-17	FT
231	(111)B			25	FT + GI
232	(111)B	8,200/51,000	6×10^{14}	15	FT
233 TG	(111)B	4,700/11,000	2×10^{15}	25	NT
234	(111)B	6,100/30,000	5×10^{15}	20	ET

TABLE II-1 (cont.)

GaAs EPITAXIAL LAYER PROPERTIES

Growth No.*	Substrate Orientation†	Mobility RT/LN $cm^2/V\text{-}sec$	Carrier Density cm^{-3}	Thickness μm	Surface Morphology‡
235 TG	(111)B	6,700/31,000	2×10^{15}	22	ET
236	(111)B	6,600/39,000	3×10^{15}	15	ET
237	(111)B	6,400/36,000	2×10^{15}	10-25	FT
238 TG	(111)B	6,111/22,000	1×10^{15}	16	NT + H
239	(111)B	7,000/36,000	4×10^{15}	10	FT
240	(111)B	6,400/34,000	2×10^{15}	15	FT
241 TG	(111)B	6,200/30,000	2×10^{15}	5-10	NT
242	(111)B	6,500/	3×10^{15}	20	FT

*All growths noted with a TG were grown in the temperature gradient cell.

†All substrates were semi-insulating unless noted as n^+ . All substrates noted with an (LD) were 15° off the (111) direction.

‡CT: coarse terraces; MT: medium terraces; FT: fine terraces; ET: extremely fine terraces; NT: no terraces; GI: gallium inclusions; H: hillocks.

Figure Captions

Figure II-1 The influence of (a) temperature gradient ∇T, and (b) rate of cooling, $\frac{dT}{dt}$, on the spatial stability of the liquid-solid interface against thermal fluctuations.

Figure II-2 Growth No. 200, demonstrating direct correlation between (a) hillocks that result from the initial stages of nucleation and (b) terraces that appear on the final growth of the layer.

Figure II-3 Growth No. 175, showing the effect of a stain on a (100) substrate surface that inhibited the nucleation of a layer. The hillocks were nucleated homogeneously in the melt and are weakly attached to the surface.

Figure II-4 Growth No. 238, (a) showing two variations of hillock formation that occurred during growth, (b) a hexagonal platelet that was homogeneously nucleated in the melt and weakly attached to the layer, and (c) a hexagonal depression in the layer that formed as a platelet grew in the melt very close to the substrate surface.

Figure II-5 Surface of a GaAs substrate after As evaporation. (a) The effect on the growth of a layer for a (111) B substrate pre-baked for 8 hours, at 750°C. The characteristic forms of the residual Ga left for the (111)B, (100) and (111)A substrates are shown in (b), (c) and (d), respectively.

Figure II-6 Typical carrier density profiles obtained from Schottky barrier diode measurements for layers on (a) semi-insulating and (b) n^+ substrates. For (a), the depletion layer extends along the surface of the substrate towards the ohmic electrode, when the depletion layer has been back biased through to the substrate. For (b), the carrier density increases abruptly when the depletion layer has been back biased to the n^+ substrate.

Figure II-7 Growth No. 232, typical of the high quality layers obtained from the horizontal tilt furnace without a temperature gradient. Note that the layer is not uniform in thickness (a); part (b) shows an enlargement of the terraces and (c) shows an etched cross section of the layer.

Figure II-8 (a) Growth No. 221, a typical sub-micron layer obtained from the temperature gradient cell. (b) Note that there are essentially no terraces, except near the small residual Ga inclusions due to substrate evaporation. The uniformity of the < 1 μm thickness is shown in the etched cross section (c).

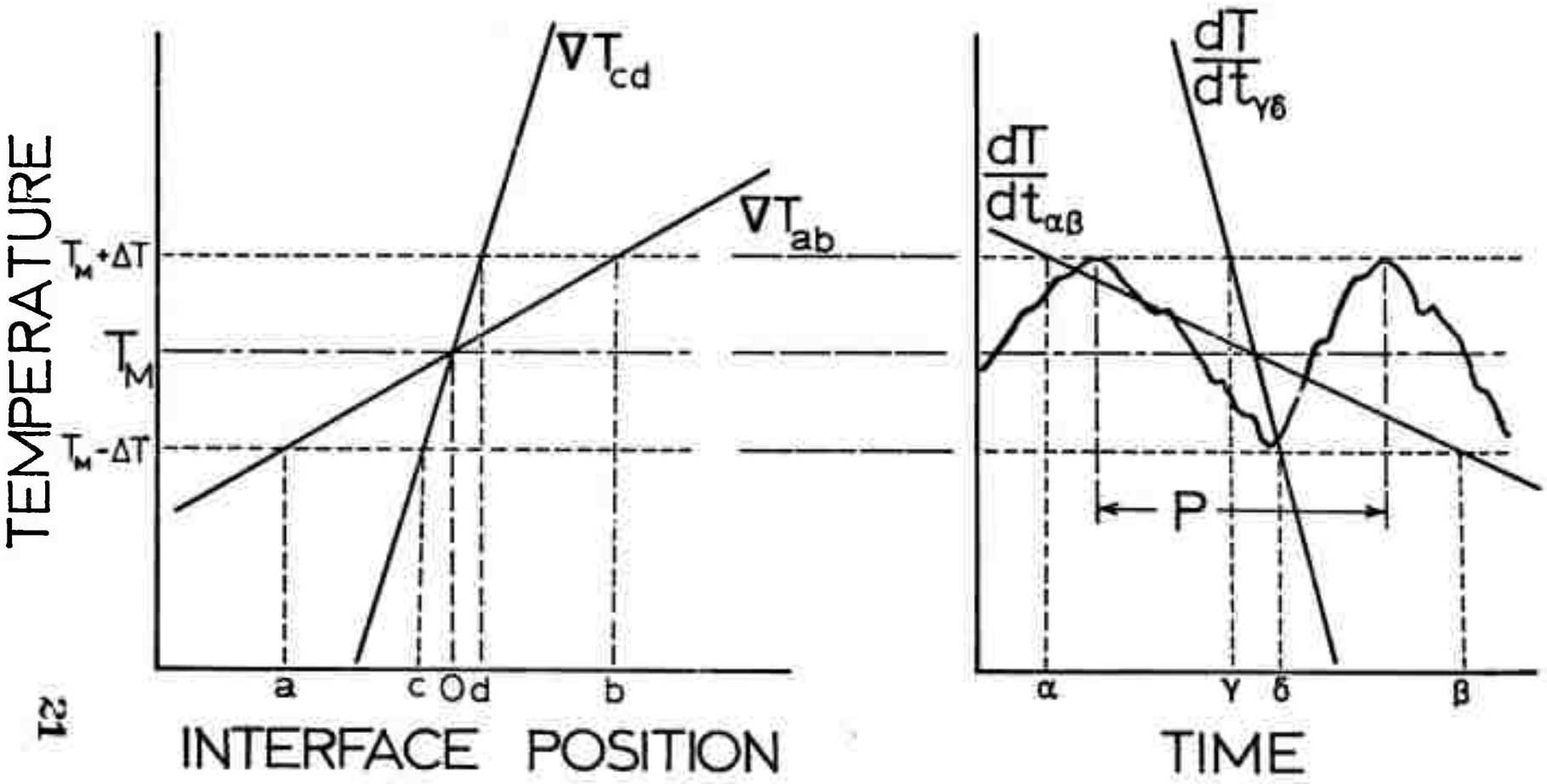

Figure II-1 The influence of (a) temperature gradient ∇T, and (b) rate of cooling, $\frac{dT}{dt}$, on the spatial stability of the liquid-solid interface against thermal fluctuations.

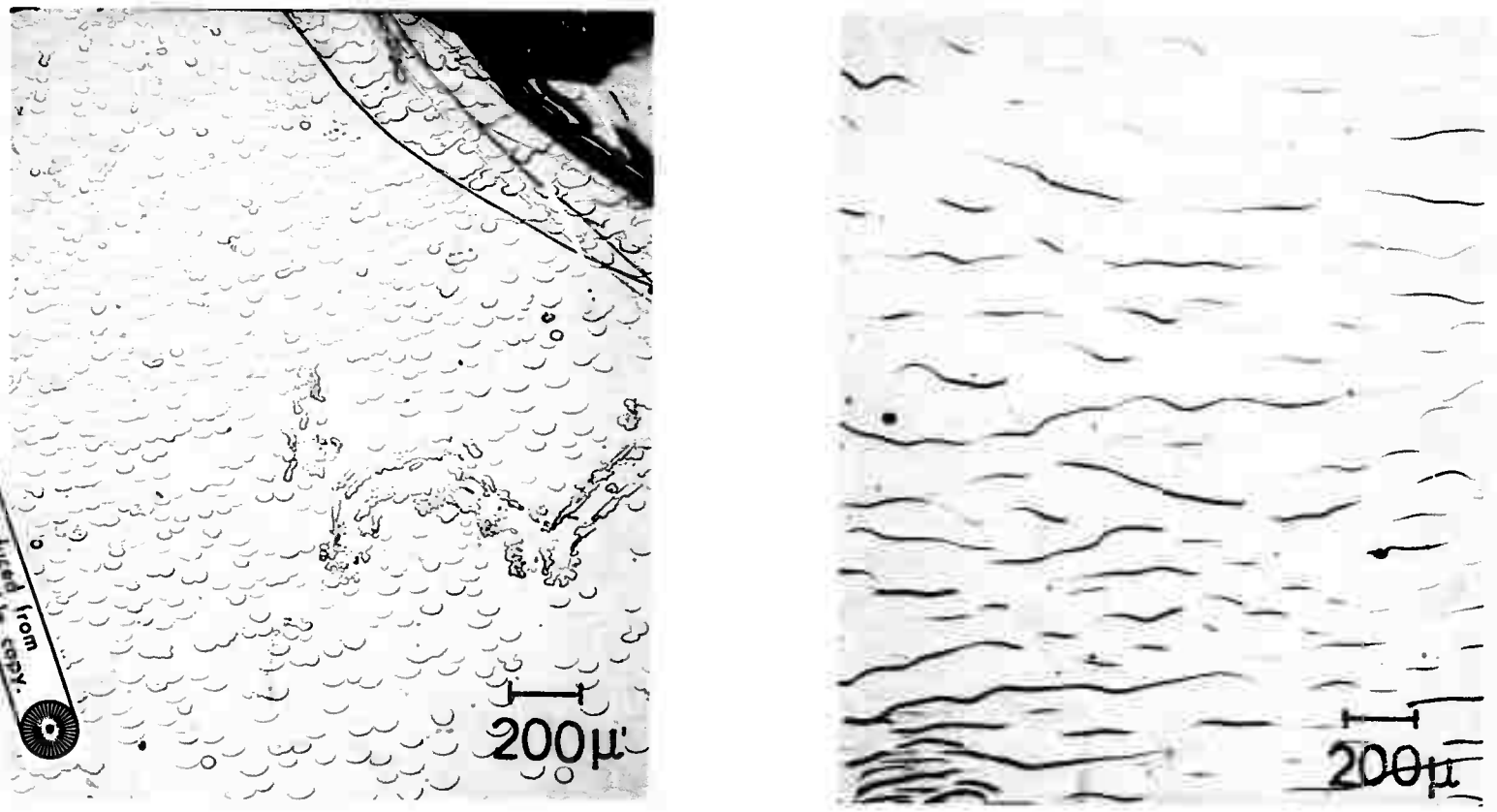

Figure II-2 Growth No. 200, demonstrating direct correlation between (a) hillocks that result from the initial stages of nucleation and (b) terraces that appear on the final growth of the layer.

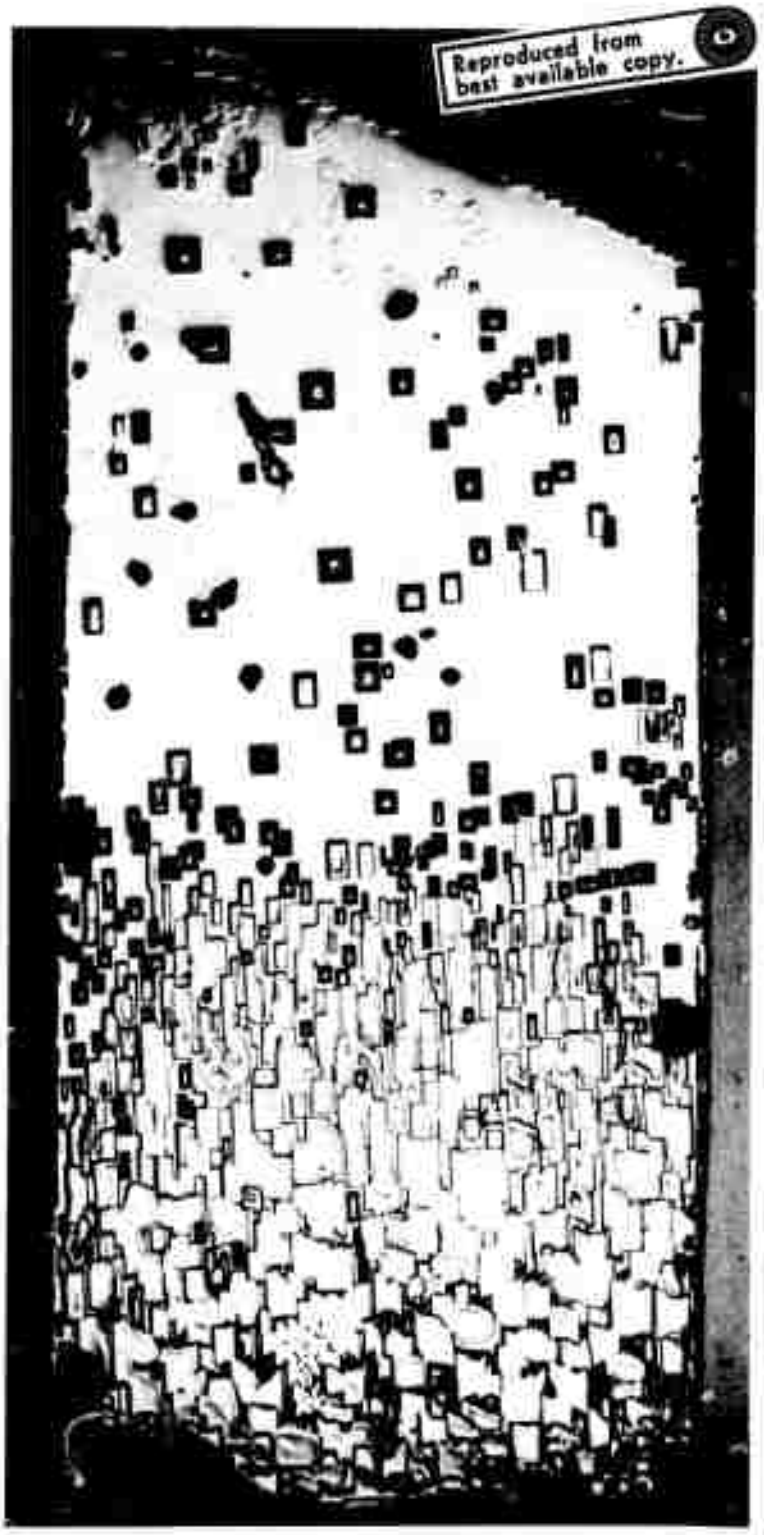

Figure II-3 Growth No. 175, showing the effect of a stain on a (100) substrate surface that inhibited the nucleation of a layer. The hillocks were nucleated homogeneously in the melt and are weakly attached to the surface.

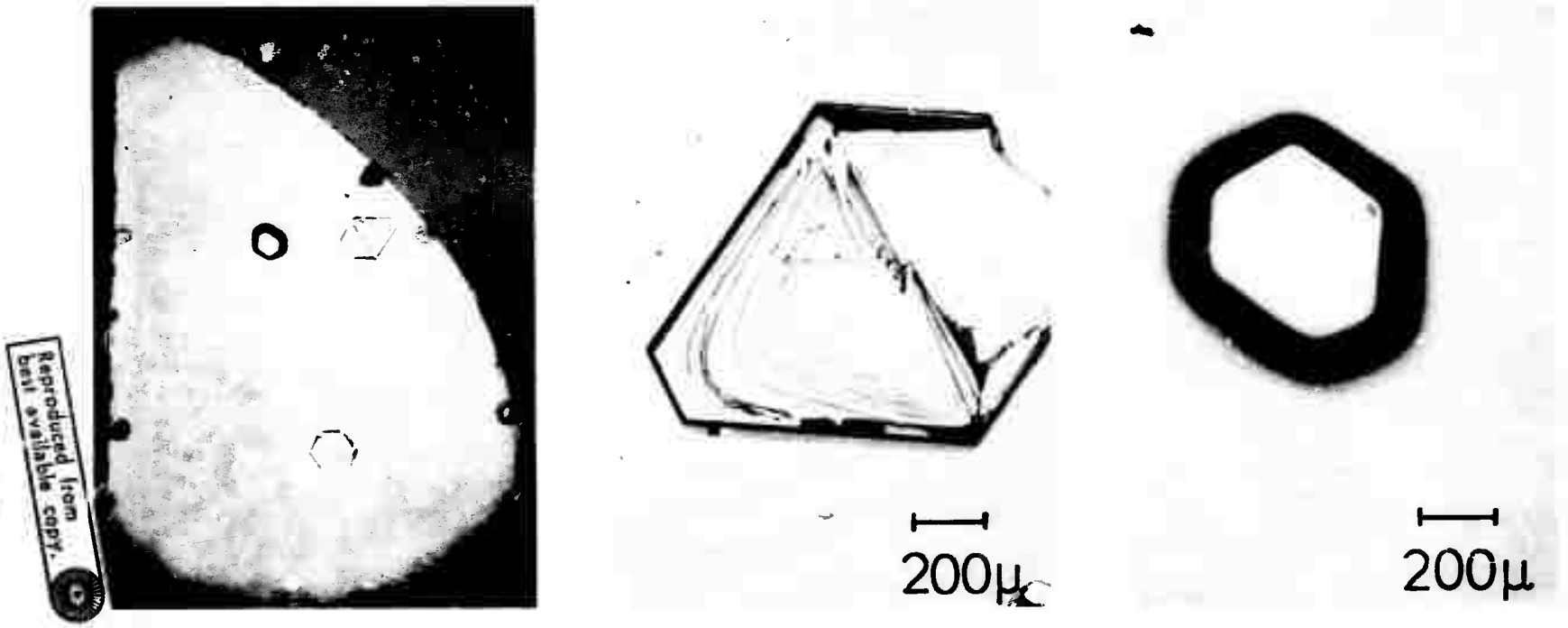

Figure II-4 Growth No. 238, (a) showing two variations of hillock formation that occurred during growth, (b) a hexagonal platelet that was homogeneously nucleated in the melt and weakly attached to the layer, and (c) a hexagonal depression in the layer that formed as a platelet grew in the melt very close to the substrate surface.

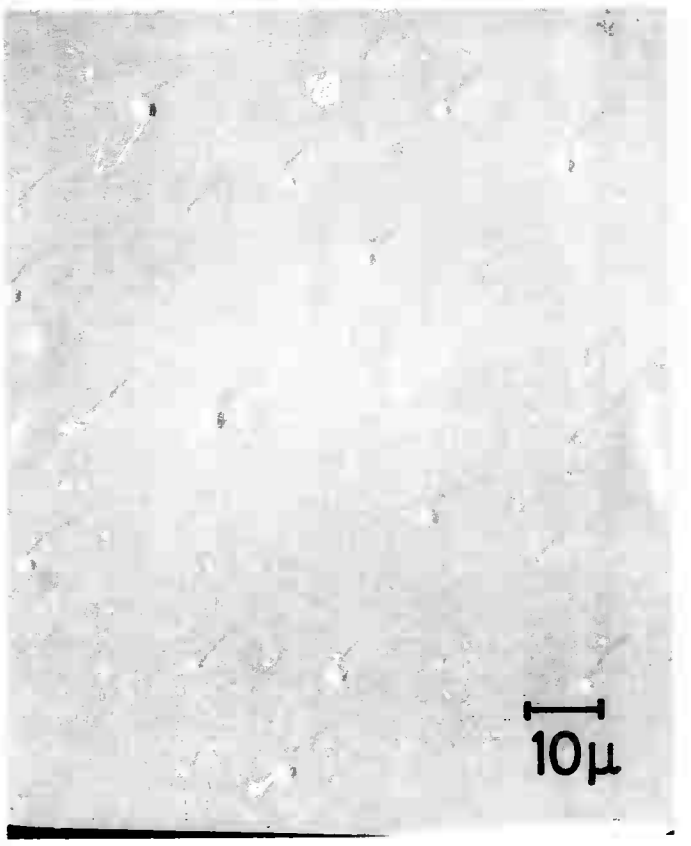

Figure II-5 Surface of a GaAs substrate after As evaporation. (a) The effect on the growth of a layer for a (111) B substrate pre-baked for 8 hours, at 750°C. The characteristic forms of the residual Ga left for the (111)B, (100) and (111)A substrates are shown in (b), (c) and (d), respectively.

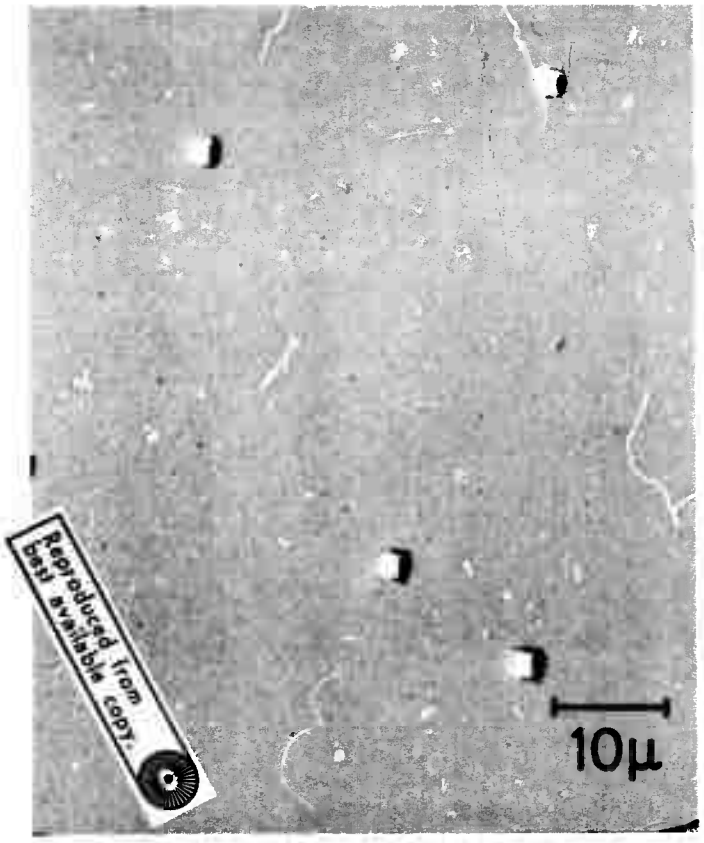

Figure II-5 Surface of a GaAs substrate after As evaporation. (a) The effect on the growth of a layer for a (111) B substrate pre-baked for 8 hours, at 750°C. The characteristic forms of the residual Ga left for the (111)B, (100) and (111)A substrates are shown in (b), (c) and (d), respectively.

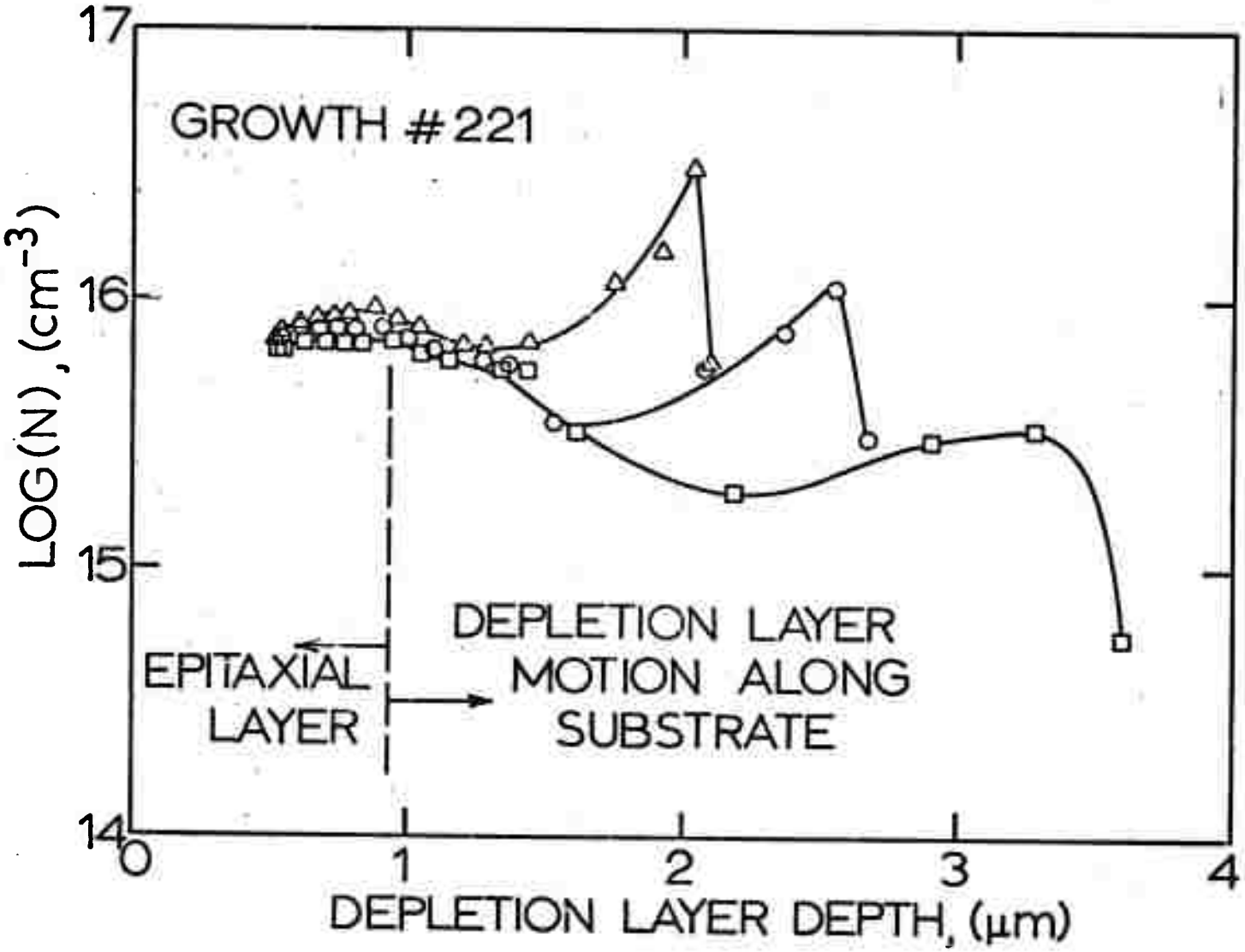

Figure II-6a Typical carrier density profiles obtained from Schottky barrier diode measurements for a layer on a semi-insulating substrate. Note that the depletion layer extends along the surface of the substrate towards the ohmic electrode, when the depletion layer has been back biased through to the substrate.

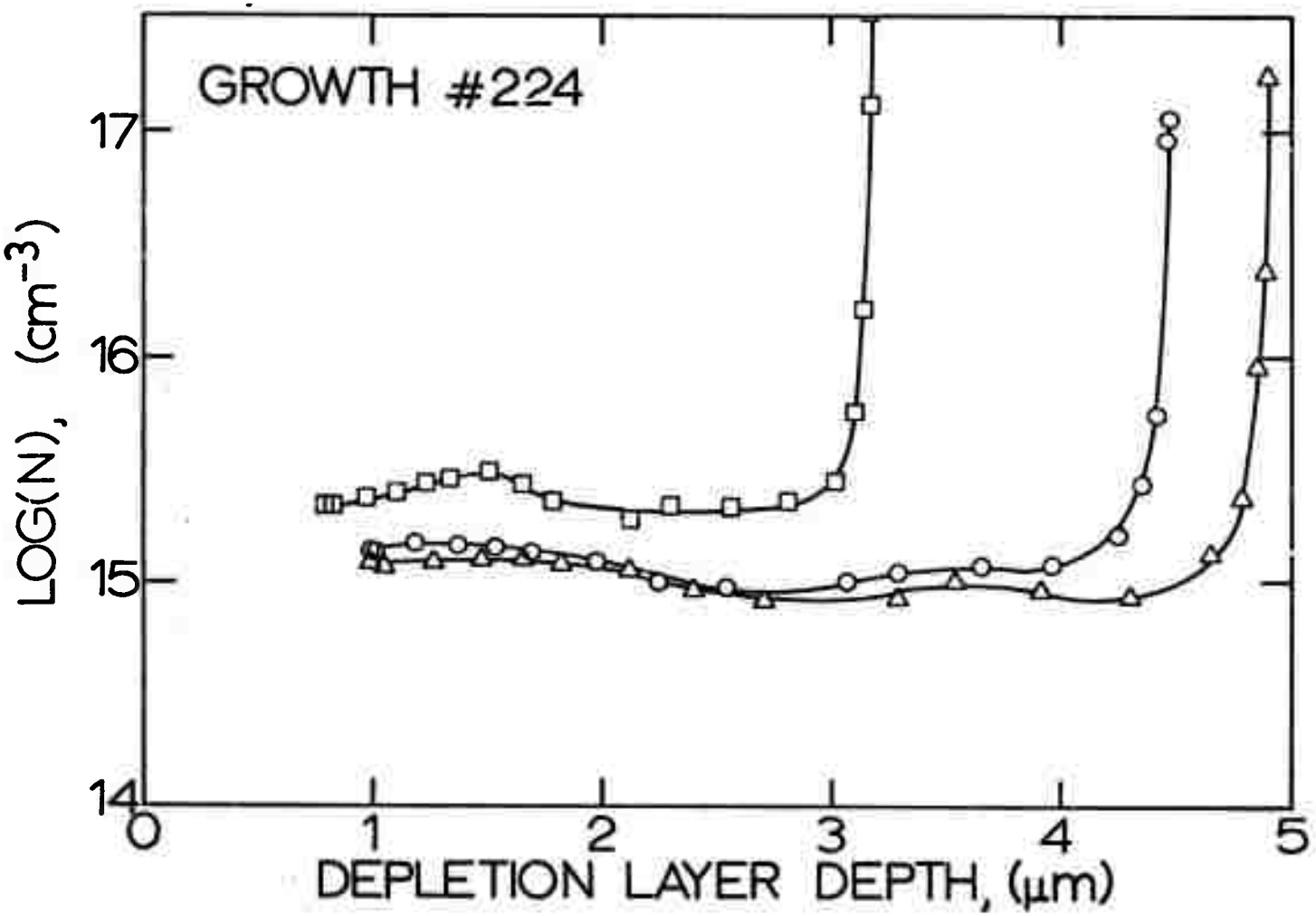

Figure II-6b Typical carrier density profiles obtained from Schottky barrier diode measurements for a layer on a n^+ substrate. Note that the carrier density increases abruptly when the depletion layer has been back biased to the n^+ substrate.

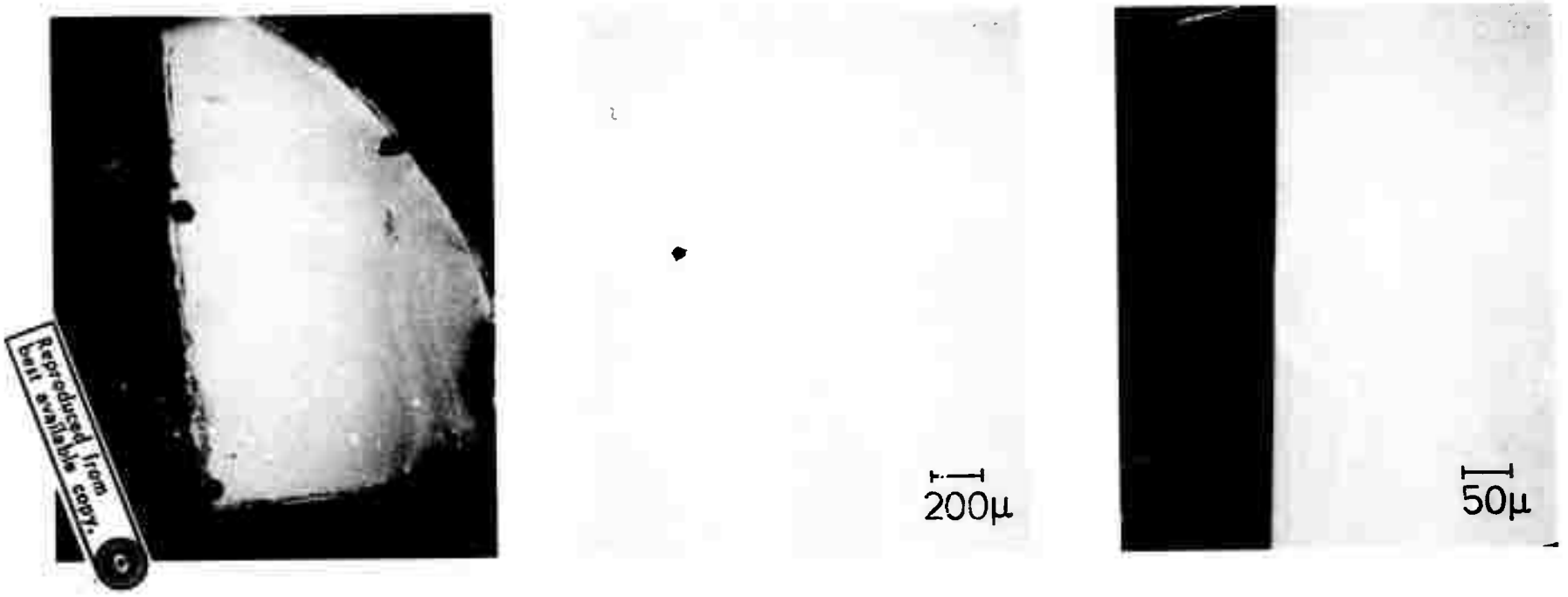

Figure II-7 Growth No. 232, typical of the high quality layers obtained from the horizontal tilt furnace without a temperature gradient. Note that the layer is not uniform in thickness (a); part (b) shows an enlargement of the terraces and (c) shows an etched cross section of the layer.

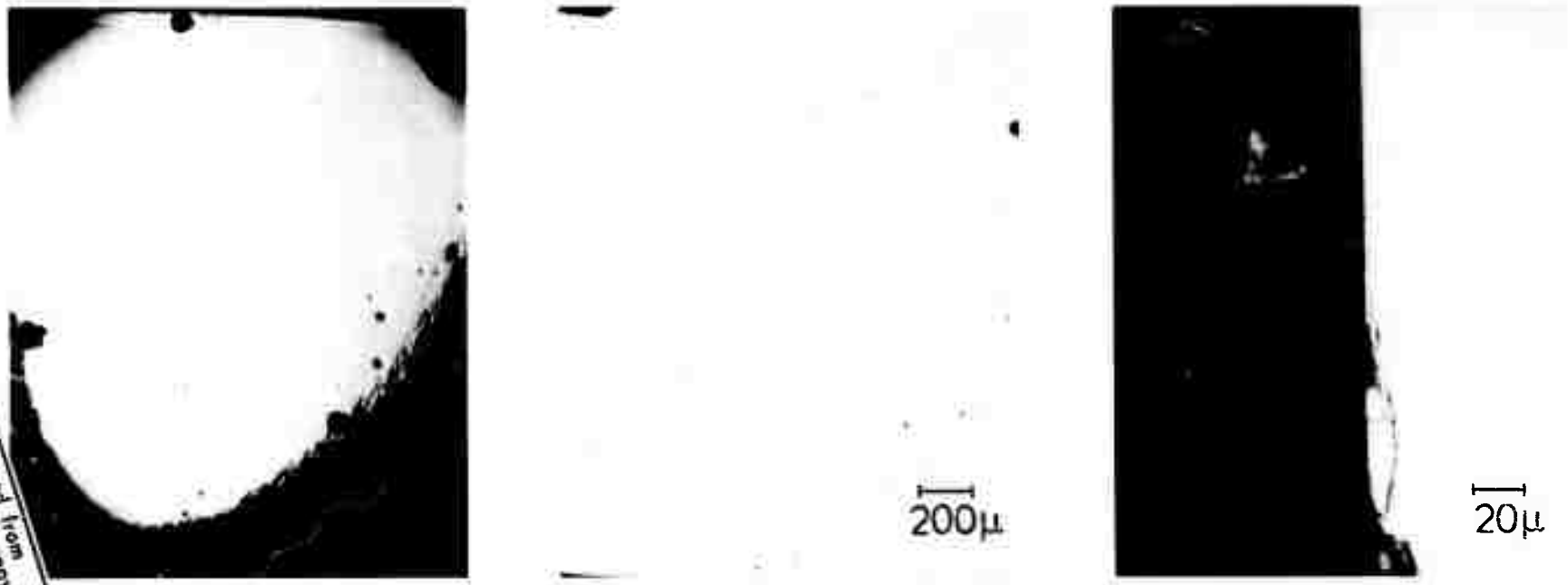

Figure II-8 (a) Growth No. 221, a typical sub-micron layer obtained from the temperature gradient cell. (b) Note that there are essentially no terraces, except near the small residual Ga inclusions due to substrate evaporation. The uniformity of the < 1 μm thickness is shown in the etched cross section (c).

III. APPLICATIONS OF COMPOUND SEMICONDUCTOR MATERIALS

G. S. Kino, C. Quate, M. Bini, G. R. Bisio,
A. Chiabrera, and S. Ludvik

A. GENERAL OBJECTIVES

The purpose of this work is to design and fabricate new and unique microwave space charge and acoustical devices. Of principal interest are planar devices in which the conduction is along a thin film of GaAs deposited on a semi-insulating substrate. The devices are fabricated using modifications of silicon integrated circuit technology. Realization of these devices requires high quality GaAs epitaxial material of specific thickness and carrier density on high quality substrates having several different orientations. These requirements are unique and hence make a closely integrated materials growth effort essential to the success of the program.

B. PROGRESS TO DATE AND FUTURE WORK

1. Gallium Arsenide Space Charge Devices

Within the last few months significant progress has been made on the unilateral space charge amplifier program, after considerable initial difficulties with the contact technology and material quality. The material requirements are typically for high quality GaAs layers 10-20 μm thick with carrier densities in the 10^{14}-10^{15} cm^{-3} range deposited on semi-insulating substrates. The material must be of very high quality in order to be resistant to avalanching in the contact regions where high fields inevitably occur. Furthermore, the substrate-active layer interface must be free of defects and impurities in order that breakdown through or along the substrate may be avoided. Finally, the surface of the epitaxial layers must be smooth enough that photomasking techniques having sub-micron resolution may be used; the devices are by necessity quite small, the width being of the order of 1 mm and the length 1 - 100 μm.

Recently a limited quantity of exceptionally high quality GaAs material meeting all three of our requirements has become available from the Center for Materials Research (CMR) crystal growth effort of this program. With this material we have been able to construct for the first time devices which show no signs of avalanche at the contacts nor any indication of substrate-interface breakdown or substrate "punch through" breakdown. Before this high quality material became available we tried epitaxial GaAs material from a number of other sources (mostly commercial but including earlier CMR growth facility material) and in no instance was the material quality high enough nor was our contacting technology perfected to the point where we could construct a diode that would saturate without oscillation and without breakdown.

We are currently using an Ag-In-Ge evaporated alloy in our photomasking procedure to make the ohmic contacts to the new high quality material. Previously we had developed an evaporated Au-Ge alloy contact and we could make good contacts to epitaxial material having $n > 10^{15}$ cm^{-3}. However for the lower density, high quality material required for the present devices, the Au-based alloy does not seem to be adequate. Part of the problem may be the fact that the Au film tends to "ball up" during the alloying step, reducing the effective area of the contact and increasing localized fields. With the Ag-based alloy this is not a problem even though the alloying temperature is higher (500°C). Using this new alloy we are now able to make very good quality ohmic contacts to the lower carrier density, higher quality material.

The goal of the unilateral space charge amplifier program is the design and construction of a solid state equivalent to the traveling wave tube for use at X band and higher frequencies. Using the empirically

measured velocity-field characteristics for GaAs, we have performed detailed calculations of the actual dc field distribution within a thin epitaxial diode. These calculations show that the dc field increases monotonically from the cathode to the anode, passing through the threshold point for negative differential mobility approximately one third of the way from the cathode for a long diode biased just above threshold. To make a successful microwave amplifier the total gain of the diode must be limited to prevent Gunn oscillations from occurring, and the input rf signal must be injected as close as possible to the threshold point at a level well above the background noise level there.

A few devices based on these calculations have been constructed. They are in the form of an insulated gate field effect transistor with two evaporated aluminum gates instead of one, as shown in Figures III-1 and III-2. The gates are capacitively coupled to the active material through a thin SiO_2 layer. The longer, grounded gate in conjunction with an active layer nd product $< 10^{12}$ (n is the carrier density in number cm^{-3} and d is the layer thickness in cm) is intended to suppress oscillations by limiting the total gain to a value of less than 50 db. The size of this electrode also determines the input and output impedances. The narrow, upstream gate is used to inject the rf signal which is then detected at the drain electrode. The narrow gate is positioned so that the input signal is injected just at the beginning of the negative differential mobility range. The total device represents the first solid state equivalent of the conventional traveling wave tube with a calculated gain of perhaps 40 db in the frequency range 8-12 GHz.

Our first devices constructed from the new epitaxial material produced very encouraging results. The source-drain I-V characteristics show very

flat current saturation with no coherent Gunn oscillations as shown in Figure III-3. Incoherent noise is emitted at voltages significantly above threshold as expected. Terminal resistances are in agreement with values calculated for the active region, showing that there is low contact resistance and that the active region thickness corresponds closely to the actual layer thickness. So far, we have not seen any gain from the initial devices because our first estimates for the best position of the input gate were incorrect and because a capacitively coupled rf input is inherently weak. The incoherent noise was observed in the frequency range 4-12 GHz, and is nothing more than highly amplified background noise. This means that the dimensions chosen were giving a little too much gain and that the input signal was not being injected at the optimum point. (It is difficult practically to locate the optimum point because of the inevitable non-uniformities in any real device.) These results are encouraging indeed, considering that this was the first test on devices in which the technology was reliable enough to give good physical measurements.

We have carried out further diagnostic tests on these devices to evaluate the quality of the material used and the nature of the field variation along them. In our experiments we used devices made from two slices of material, slice I with $n = 8 \times 10^{14}$ cm^{-3}, $\mu \sim 8000$ $cm^2/V\text{-sec}$, thickness $d \approx 10$ μm and slice II with $n = 3 \times 10^{14}$ cm^{-3}, $\mu \approx 8000$ $cm^2/V\text{-sec}$, thickness $d \approx 10$ μm . All devices were 70 μm long with the longer gate 35 μm long, the shorter gate 5 μm long and 5 μm spacing between gates and contacts. With sample I, due to alignment problems, the spacing between the long gate and the drain in the final device was 10 μm . Typically we made approximately 9 devices at a time (three rows of three) on a substrate. The contacts were good in all but 1 out of 18 devices (a device near the edge

of the substrate). Some of the smaller gates, 5 μm wide, had breaks so that the yield was 5 good devices of type I and 4 of type II.

The threshold voltages for onset of noise and for saturation seemed to be very consistent between all devices of type I, and lower than for devices of type II which were again consistent among themselves. However, the threshold current and the low field resistances of the devices did vary from one to the other by as much as 20%. We believe that this is due to nonuniform thickness of the epitaxial layer rather than contact problems.

We have carried out preliminary measurements to obtain some indication of the field variation along the devices. We leave the gates floating and measure the induced voltage on them with a high impedance probe when a short pulse is placed across the source and drain electrode. This gives an indication of the average potential at each gate. As expected the field is higher on the drain side of the device than near the source, when the average field is above threshold. We intend to improve this technique by decreasing the stray capacities so as to be able to obtain more complete diagnostic measurements of the devices.

We have operated these devices so far on a pulsed basis rather than dc, because the power dissipation is of the order of 2 watts. An increase in the duty cycle tends to lead to excessive heating. However, at no time have we experienced problems with breakdown of the semiconductor material or contacts up to the point of melting. The only breakdown problems in pulsed devices have been due to breakdown in the SiO caused by application of excessive voltages.

Several modifications based on these observations are being incorporated into the next set of devices already under construction. First, the active region will be half the length of the present set. New photomasks

have already been made for this purpose. This should lower the gain and hence the rf output noise, and it should reduce the dc power dissipation to a point where we may be able to operate on a dc basis. Eventually we would hope to obtain CMR material having a thickness of only 5 μm. This should entirely eliminate the dc power dissipation problem. Furthermore, the second generation of devices will make use of Schottky barrier aluminum gates instead of SiO_2 insulated gates. This should have the dual advantage of giving better control over the dc field in the gate region and improving the rf coupling of the input gate.

2. Gallium Arsenide Acoustic Devices

a. Linear Amplifiers

Within the past few months we have made a major advance in using GaAs to amplify acoustic waves. The need for amplifiers comes about through our program of fabricating very long delay lines by folding an acoustic path forth and back on a given crystal. As the total delay increases it is necessary to resort to amplification to overcome the intrinsic losses. Previous work on bulk acoustic waves has shown that amplification is readily obtainable in GaAs since the crystal is piezoelectric. However, with bulk modes the problem of heat dissipation proved to be insurmountable and we have not pursued this work beyond the initial fundamental studies. Recently, we have been measuring the properties of Bleustein[1] waves propagating along the $\langle 110 \rangle$ axis near the surface of a crystal with $\langle \bar{1}10 \rangle$ normal to the surface. These waves possess the special property of rather slow exponential decay in the direction normal to the surface, and thus they extend a rather large distance into the bulk. This is in contrast to the Rayleigh surface waves which decay very rapidly into the crystal and, therefore, only have appreciable strength near the surface. For amplification of Rayleigh waves

it would be necessary to use a thin layer of drifting electrons at the surface. The inherent surface states associated with this kind of current has made it difficult to amplify the surface waves directly. The Bleustein wave apparently combines the desirable properties of bulk waves with those of the Rayleigh wave; that is, the rate of decay into the bulk is slow enough that there is a large interaction with the electrons far from the surface but yet the peak strength of the field is at the surface so we can use surface wave techniques to launch and detect the waves. Thus, in our experiments on the amplifier we have used surface interdigital transducers to launch and detect the wave between the input and the output. We have fabricated ohmic contacts on the surface and with a dc field between them we have been able to achieve 90 dB of gain in 1 cm for a frequency near 300 MHz. These values are rather similar to what we obtained previously with bulk waves, and we believe that we are measuring interactions that are determined by the fundamental piezoelectric coupling between the wave and the drifting carriers. Much of our work has been with oxygen doped crystals. Since, however, the gain is in excess of what we need, it is clear that epitaxial layers on semi-insulating substrates would also form an excellent system for propagating and amplifying Bleustein waves.

In this report we describe the amplification characteristics for the surface shear wave in GaAs where the propagation direction (x-coordinate) is along the $\langle 110 \rangle$ direction on the $(\bar{1}10)$ surface. Here, the particle motion is along the $\langle 001 \rangle$ direction and the dispersion relation for the partial waves $\left| \sim e^{-rkz} \cdot e^{j(\omega t - kx)} \right|$ is found from the stiffened Christoffel equation[2] to be:

$$\frac{v^2}{v_B^2} = (1 - r^2) + \frac{K^2(1 + r^2)^2}{(1 - r^2)} \qquad (1)$$

The material for these experiments was O_2-doped GaAs with a room temperature resistivity around 6×10^3 Ω-cm and Hall mobility of 6500 $cm^2/Vsec$, provided by the Monsanto Company. The resistivity could be conveniently changed over three orders of magnitude by heating the sample from room temperature to around 200°C. The Hall mobility in the same temperature range changed only by about 30%. One disadvantage of this approach is that ohmic losses due to conduction between finger pairs increase, however, it was found that the zero field transmission loss (Figure III-4b) passes through a peak with increasing temperature. This indicates that the acoustic transmission loss dominates. At room temperature, by using a rectifying barrier for the transducer electrodes it was possible to obtain an overall tuned loss, with no drift field, of 45-50 dB over a propagating distance of 1.1 cm.

In Figure III-5, we show a series of gain vs drift field curves for different temperatures of a 5 mm drift section with field varied between ± 1.2 kV/cm. The gain is specified relative to the zero field value so that the effect of the change of individual transducer efficiency with temperature is eliminated. The behavior of the gain is typical of that found in bulk wave amplifiers in both CdS[4] and GaAs.[5] In the forward direction the gain exhibits a shallow maximum while in the reverse direction the characteristic is considerably sharper. We note also that the point of minimum gain shifts away from zero field at higher temperatures, and the gain curve becomes more symmetric.

The results found here may be described quite well in terms of the theories developed by Hutson and White,[3] Uchida et al,[6] and Greebe,[7] where the effects of trapping centers on the acoustoelectric interaction are taken into account. In addition to the resistivity and mobility variation with

temperature, the other parameters needed are the trapping factor (f_0) which represents the fraction of the total rf space charge associated with mobile carriers, and the trapping time (τ) of the centers which contribute to the bound space charge. The theoretically calculated curves shown in Figure III-5 have been obtained from the gain expression of Uchida et al.,[7] using measured values of pulsed resistivity and Hall mobility at the different temperatures. For each instance, the trapping parameter (f_0) is varied using a fixed value of trapping time ($\omega\tau = 0.2$). The amplification characteristics over other drift regions of the sample showed variations as much as 5 - 10 dB/cm at the higher fields values and this can be attributed to inhomogeneities in the resistivity of the specimen of 30-40% which is not uncommon for the O_2 doped material. Measurements on the third harmonic (615 MH_z) of the transducer have indicated gains in the vicinity of 75-80 dB/cm, however the signal in this case could only be observed with the drift field applied since the transducer efficiency was very low at this frequency. Other evidence for these large gains at the high temperatures ($\geq$ 100°C) can be found in the appearance of current saturation effects, typical of acousto-electric oscillation. The onset time for this saturation is around 10 μsec which is consistent with acoustic delay times associated with the sample.

The good agreement of the amplification characteristics with theory demonstrates the applicability of the bulk wave description and confirms the results found for the related surface shear mode found in CdS.[8] The importance of the high mobility available in GaAs is clearly significant where we find the peak gain occurring at fields around 800 V/cm. It has been possible to operate this amplifier with a dc drift field to obtain a relative gain of 15 dB by relying on the resistive heating to change the carrier concentration. The gain was limited by the maximum drift field

($\leq$ 300 V/cm) which is dependent on the sample thickness and heat sink conditions. We have also done some initial experiments using bulk wave transducers to excite these waves and the success of this work indicates that we may be able to go to much higher frequencies than are possible with interdigital transducers.

In summary, the magnitude of the gain measured in high resistivity O_2 doped GaAs is more than adequate for loss compensation in delay line structures. Hence it is clear that epitaxial layers on semi-insulating substrates would also form an excellent system for propagating and amplifying Bleustein waves. And because they can be made much thinner than bulk material, they would offer the great advantage of lower dc power dissipation, making possible dc operation under conditions of maximum acoustic gain. We therefore feel that we have developed a system using the amplification of Bleustein waves which will allow us to use the epitaxial crystals grown in the CMR facility to construct a number of new devices which should have significant device applications.

b. Nonlinear Acoustics

On another program we have been studying, for the past two years, the nonlinear interaction between two acoustic surface waves traveling in opposite directions on the surface of a crystal. On these nonlinear devices we can measure an output which is proportional to the product of the two traveling waves. The devices that result from this provide us with a means of doing convolution in real time, performing pulse compression on wide band radar signals, implementing new pattern recognition devices, and imaging optical waves through acoustic scanning of semiconductor surfaces. In the past we have made use of silicon films placed adjacent to lithium niobate crystals. With the availability of good GaAs crystals, we should

now like to study nonlinearities associated with the electron conduction in this material. We would propose to construct a rather extended Schottky barrier on the surface with a reverse bias and propagate two surface waves through this region and in such a direction that the electric fields associated with the acoustic waves will enhance or decrease the biasing field. The non-linearity associated with reversed bias junctions is one of the largest known. Implementing this on a traveling wave bias will allow us to perform a convolution action in real time with all its attendant virtues. The large magnitude of the nonlinearity will give us a much greater signal at the output for a given input. Since this is a major limitation of the present devices we can foresee a significant advance in the system using the reversed bias barrier on GaAs layers.

c. Interaction of Gunn Domains with Acoustic Waves

With the advent of high-quality epitaxial layers on semi-insulating substrates that exhibit a high degree of resistance to avalanching we can now initiate a program of device research aimed toward the exploitation of Gunn domains and acoustic waves. The properties of Gunn domains in GaAs have been critically examined and presented in the literature and their features are now rather well known. We are particularly interested in one aspect of this recently discussed by Yania[8] of the University of Tokyo wherein they generate a single domain of a known shape in an epitaxial layer of GaAs on a semi-insulating substrate. The domain was triggered with a small electric signal applied to a gate electrode near the cathode. Since GaAs is piezoelectric, there is a large acoustic field associated with the Gunn domain and some of the properties of the acoustic wave generated by this mechanism have been measured both here at Stanford and in Japan. We can visualize this technique as a method of generating a short pulse of acoustic

energy which propagates along the surface of a crystal. This pulse can be amplified by the method described previously. The final part of our scheme would be to use the electric fields associated with the amplified acoustic pulse to trigger a Gunn domain at the output. That is, near the output we would have a cathode-anode region biased near the threshold of Gunn oscillation and replace the triggering gate electrode that was used to initiate the single Gunn domain at the output by the electric field associated with the large amplitude acoustic pulse. In this system then, we visualize the following mode of operation. An electrical pulse of small amplitude on the input gate would trigger a Gunn domain of known amplitude and shape. In turn, the single domain would generate an acoustic pulse which could freely propagate down the length of the delay line. In the course of this propagation it would be amplified to a level where it could initiate a single Gunn domain in the output section. This Gunn domain could then be used either to trigger a second impulse in a cyclic operation or it could be detected directly as the output. In any event, it is important to note that its shape and amplitude are fixed by the properties of the GaAs crystal. Therefore, we would have a system for "regenerating" the pulse that we started with and thus eliminate any distortions that would occur to the acoustic pulse during the course of its propagation through the delay line. We believe that this device could be used to perform a number of useful functions.

REFERENCES

1. J. L. Bleustein, Appl. Phys. Letters 13, 412 (1968).
2. B. Auld, "Microwave Acoustics," John Wiley (1972).
3. A. R. Hutson and D. L. White, J. Appl. Phys. 33, 40 (1962).
4. Y. Kichuchi, N. Chubachi, and K. I. Inuma, IEEE Trans. SU-16, 189 (1969).
5. F. S. Hickernell, IEEE Trans. SU-13, 73 (1966).
6. I. Uchida, T. Ishigur, Y. Sasaki, and T. Suzuki, J. Phys. Soc. Japan 19, 674 (1964).
7. C. A. A. J. Greebe, IEEE Trans. SU-13, 54 (1966).
8. International Electron Device Conference, Washington D. C., October 1971.

Figure Captions

Figure III-1 (a) A schematic of a GaAs amplifier. (b) The circuit used with the device. (c) A top view of the GaAs amplifier presently being constructed.

Figure III-2 (a) Photos of a completed traveling-wave Gunn Amplifier constructed from material grown at Stanford. (b) A photo of the active region showing the gate spacing, etc.

Figure III-3 Typical I-V characteristic showing flat current saturation and incoherent noise above threshold value. Diode 222-4. Horizontal scale 5 V./division, vertical scale 10 mA/division.

Figure III-4 (a) Schematic diagram of amplifier arrangement and crystal orientation. (b) Zero field transmission loss as a function of temperature showing combined transducer ohmic loss and propagation loss.

Figure III-5 Acoustoelectric gain versus drift field for a number of temperatures, compared with theory. Coupling constant (K^2) = 0.005 .

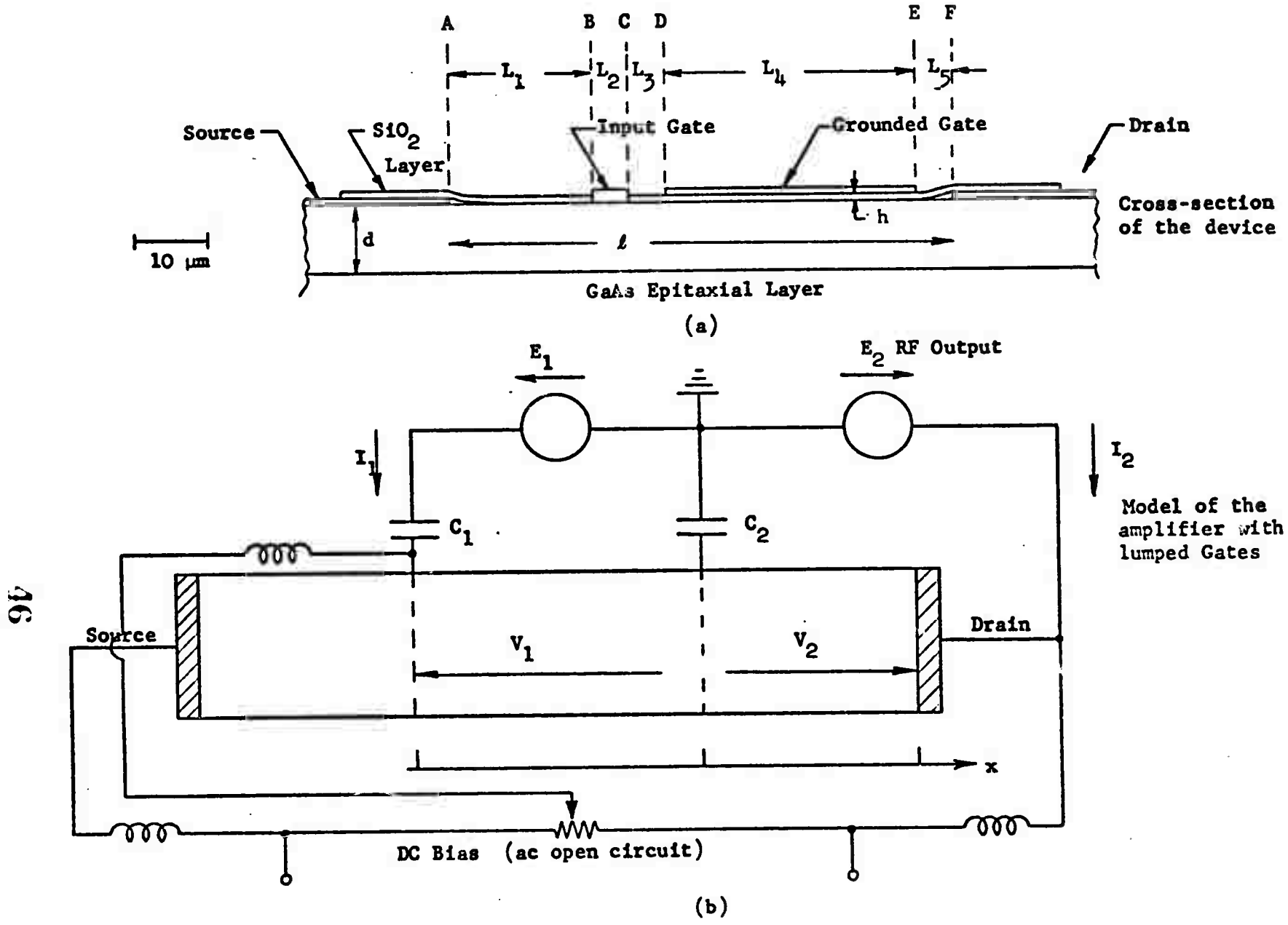

Figure III-1 (a) A schematic of a GaAs amplifier. (b) The circuit used with the device. (c) A top view of the GaAs amplifier presently being constructed.

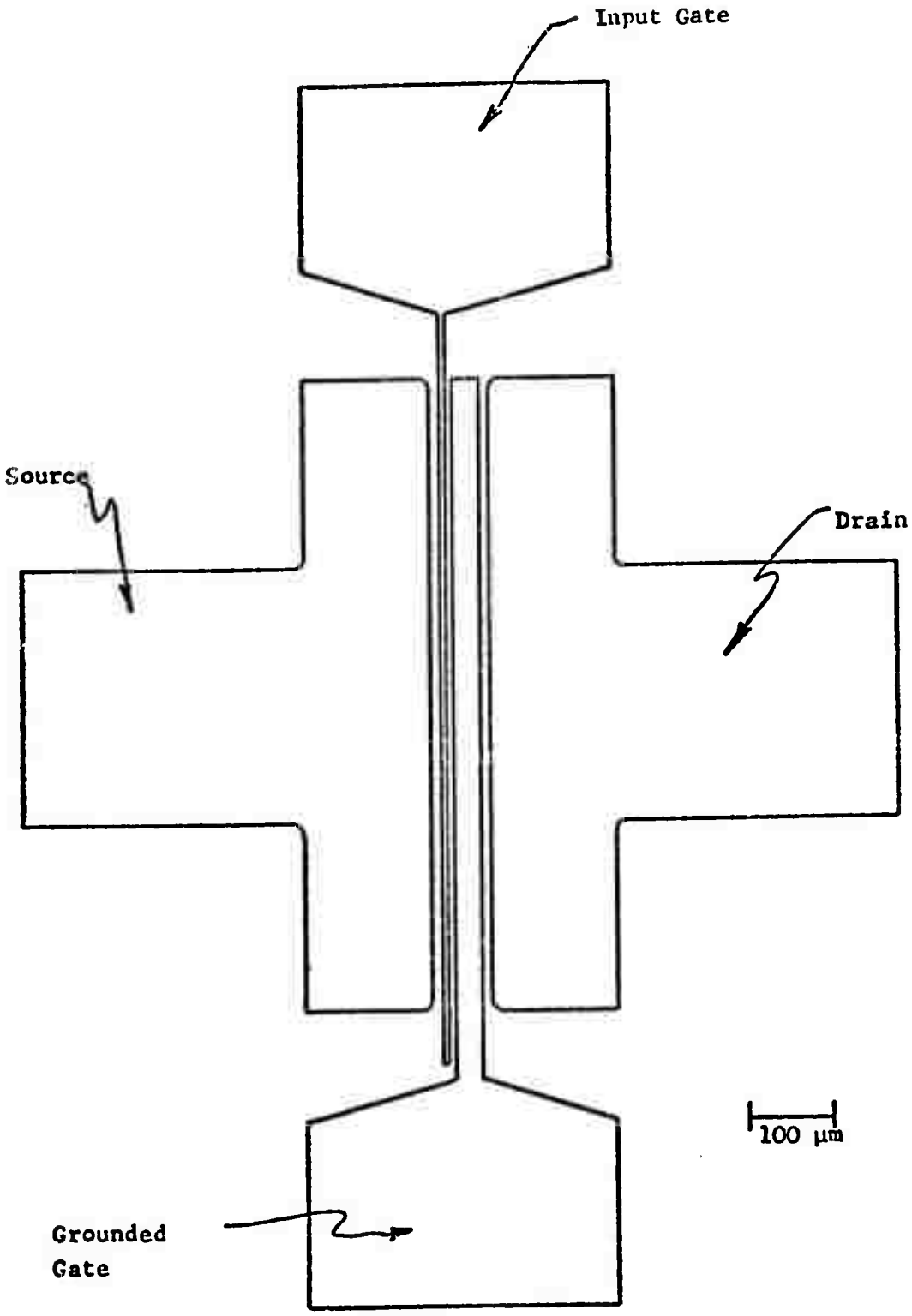

Figure III-1 (c) A top view of the GaAs amplifier presently being constructed.

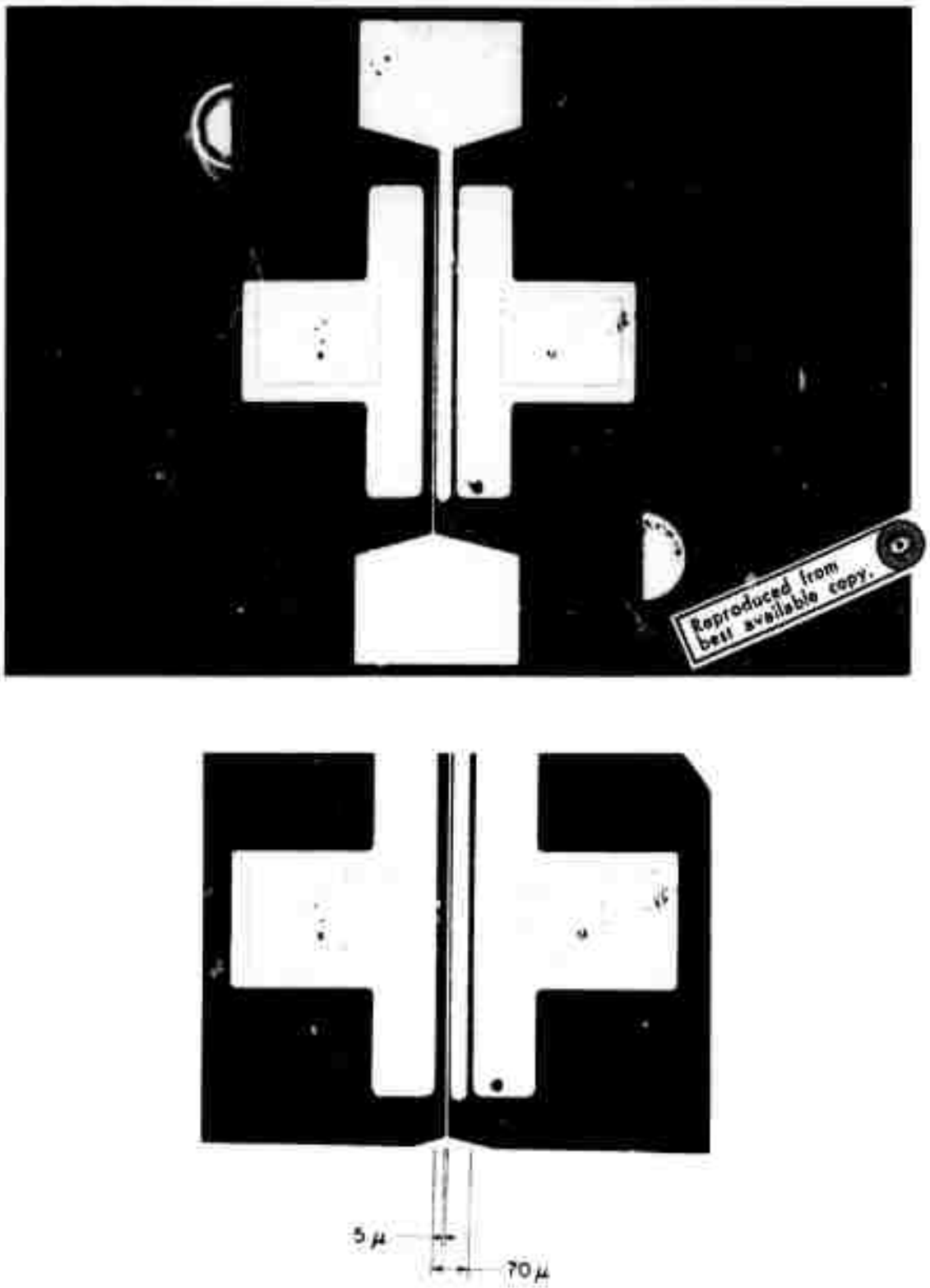

Figure III-2 (a) Photos of a completed traveling-wave Gunn Amplifier constructed from material grown at Stanford. (b) A photo of the active region showing the gate spacing, etc.

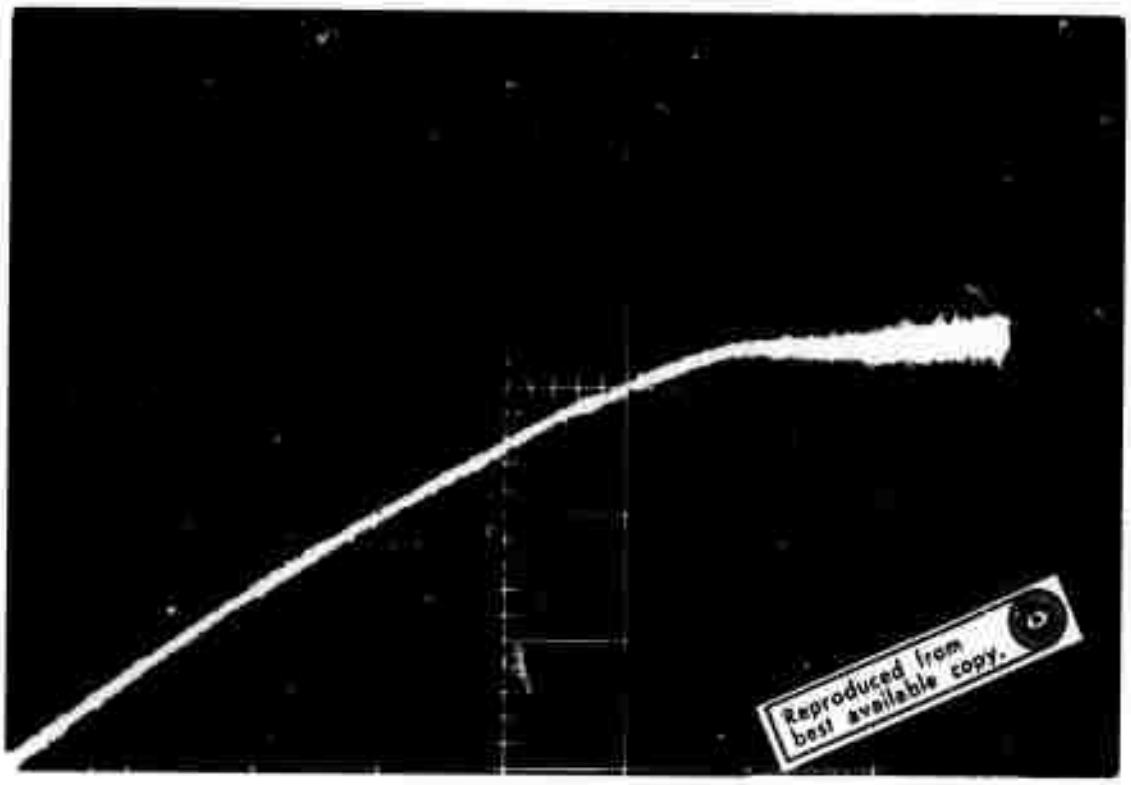

Figure III-3 Typical I-V characteristic showing flat current saturation and incoherent noise above threshold value. Diode 222-4. Horizontal scale 5 V./division, vertical scale 10 mA/division.

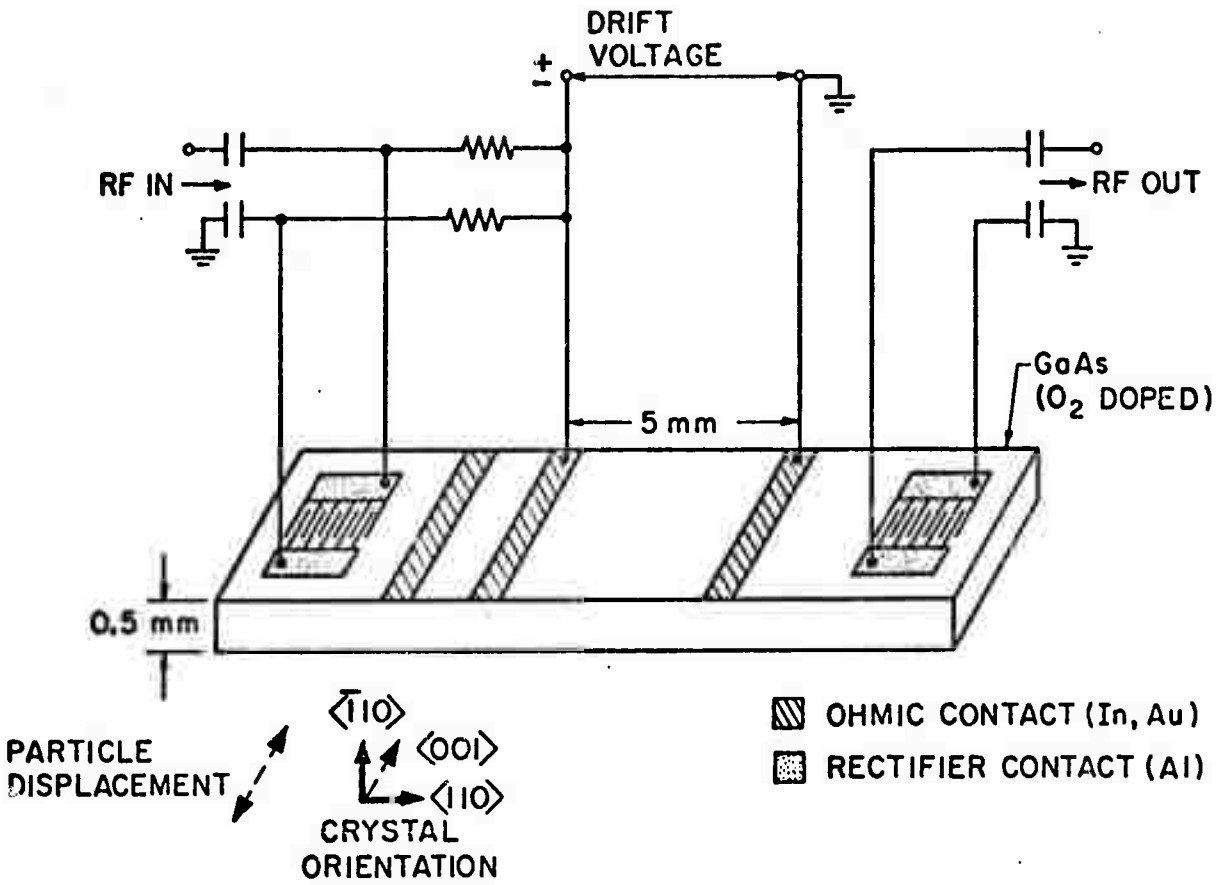

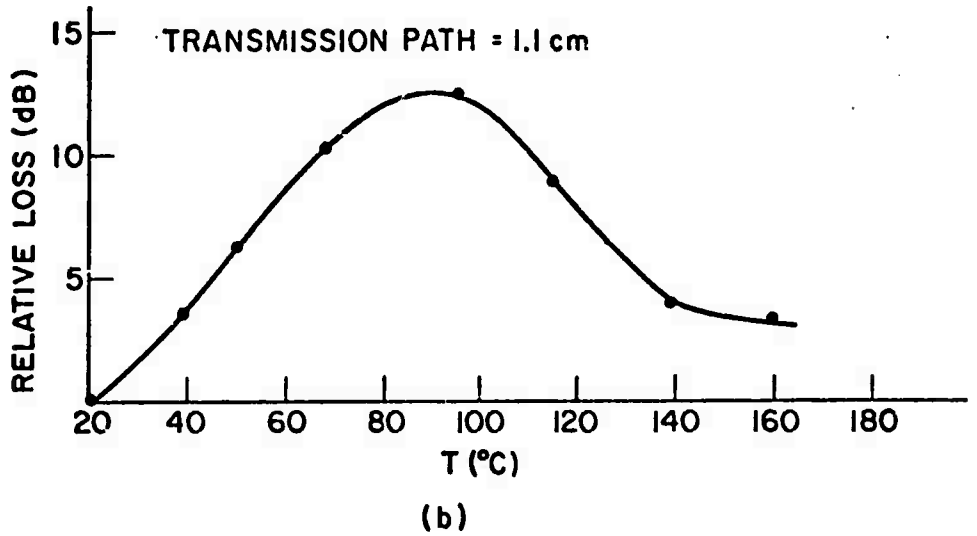

Figure III-4 (a) Schematic diagram of amplifier arrangement and crystal orientation. (b) Zero field transmission loss as a function of temperature showing combined transducer ohmic loss and propagation loss.

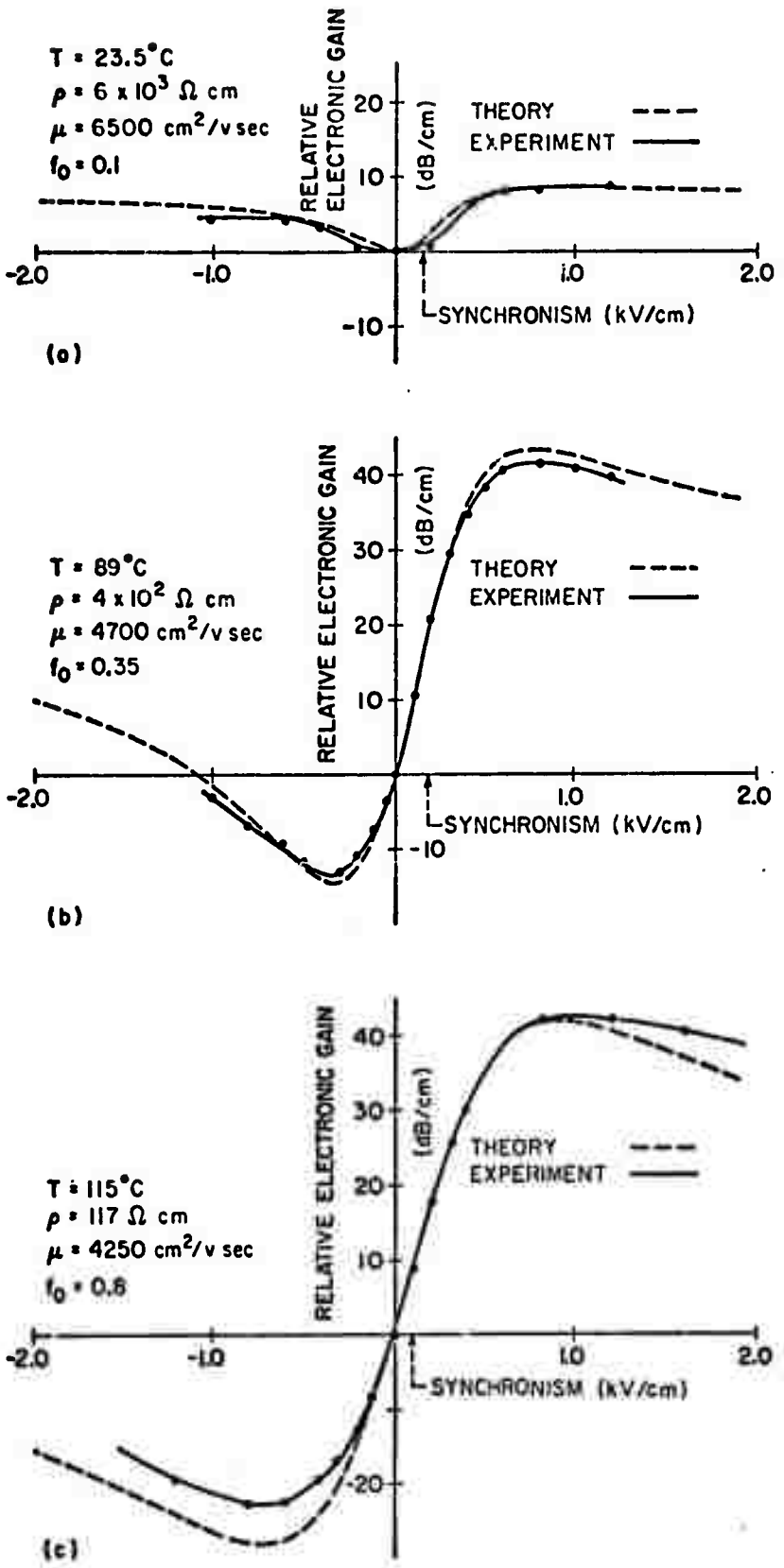

Figure III-5 Acoustoelectric gain versus drift field for a number of temperatures, compared with theory. Coupling constant (K^2) = 0.005 .

IV. PRECIPITATION STUDIES IN COMPOUND SEMICONDUCTORS

D. A. Stevenson and W. C. Rhines

A. PROGRAM OBJECTIVES

The occurrence of precipitation in compound semiconductors is of practical interest because of the influence on the electrical and optical properties. The precipitation of electrically active foreign atoms may cause a disparity between the bulk concentration of foreign atoms and the concentration of foreign atoms that are in solution. If local distortion of the lattice accompanies precipitation, then changes in dislocation density may accompany the precipitation process. In addition, the mere presence of a dispersed precipitate will modify the electrical transport and optical properties of semiconductors. The question of the extent of precipitation, the nature of the precipitate and the mechanism of precipitation are questions of practical relevance.

Precipitation in zinc vapor-doped GaAs has been the major topic of study to date and was selected because of its relevance to devices and the conflicting reports in the literature on the characteristics and identity of precipitates in this system. The major emphasis in this study has been the use of transmission electron microscopy. The progress in the last months is described below.

B. PROGRESS

Types of Precipitates Observed

During the report period, 20 variations in diffusion conditions for Zn in GaAs have been introduced. The precipitates produced in each case have been examined using electron microscopy of (100) oriented foils, fabricated using a modified jet polishing technique.

Nearly all precipitates observed have a Widmanstätten orientation to the GaAs matrix and are either: (1) faceted, apparently in the form of 18-sided polyhedra, with no evidence of strain fields (Figure IV-1), or (2) precipitates showing matrix contrast with symmetric strain fields (Figures IV-2 and IV-3).

The first type of precipitate is by far the most commonly observed in diffused samples. Though these precipitates appear to exhibit only "structure factor contrast" (more electron scattering than that of the matrix indicating greater electron density in the precipitate), it is possible that the darkness of the precipitates is caused by diffraction contrast (a different orientation of the precipitate material from the GaAs matrix) and that we have been unable to detect any diffraction spots from the precipitates because of their very low volume percentage. If matrix distortion exists only in directions perpendicular to the diffusion front in these precipitates, then it would not be visible in the photographs.

The second type of precipitate is usually seen as in Figure IV-2, with two lobes characteristic of a radially symmetric strain field. In cases where the strain field is more clearly resolved, and where precipitates with no matrix contrast appear beside those with contrast (Figure IV-3), it seems that the precipitates are all oriented identically, with the "lines of no contrast" in the strain fields running diagonally across the precipitates.

Precipitate and Dislocation Distribution

In most GaAs samples, heavily doped from a limited, pure Zn source, the precipitates are fairly uniformly distributed (Figure IV-4). It is conceivable, though not certain, that all the precipitates lie along dislocations, since only the dislocations oriented properly with respect to

the electron beam will exhibit the contrast necessary to show up in the pictures. All dislocations which do appear are pinned in one or more places by precipitates, but it is not known whether the precipitates or dislocations formed first.

In addition to the type of dislocations seen in Figure IV-4, lines of contrast which could be misfit dislocations, are seen in almost all samples annealed above 600°C. (Figures IV-5 and IV-6.) Misfits have been predicted to form in Zn-diffused GaAs because of the steep diffusion front, which causes a rapid change in lattice parameter from the diffused material, which is expanded to accommodate the Zn, to the undiffused GaAs. Theoretical predictions also indicate that the lines of misfit dislocations will exhibit square symmetry when viewed along <100> directions and that the misfits will follow <110> directions. Strangely, however, the spacing of the "misfits" in Figures IV-5 and IV-6 is about 1μ, instead of the 10μ predicted by theory and observed through etching and x-ray topography by previous investigators.[1,2] In addition, these "misfit-like" lines were observed in one control sample which was annealed with no Zn diffusion source, indicating that they were caused by impurity diffusion, thermal stresses, or polishing effects.

Since etched cross sections of the GaAs after diffusion always show very planar diffusion fronts, which may delineate the precipitation zone, a number of crystals were cut so as to examine the GaAs inside the diffusion zone as well as ahead of it. Examination of samples taken from the region ahead of the diffusion front shows no precipitation but, in many cases, the "misfit-like" lines of contrast appear. Within the diffusion zone, precipitates and "misfit-like" lines always appear (with one exception, noted later). In samples near the edge of the diffusion front, but on the diffused

side, precipitates become rare and appear usually along dislocations in fairly straight lines (Figures IV-7 and IV-8). Matrix strain around precipitates is more common in this region (Figure IV-9). These observations may be indicative of the character of the precipitates during the early stages of formation. Several attempts have been made to obtain electron microscope samples which expose the actual diffusion front. This has been done by angle lapping the specimens before final thinning but, thus far, the samples have shown little, if any, gradation in precipitate density, probably due to the difficulty of intersecting the diffusion front at the thinnest part of the specimen. These efforts will be continued in the future.

Precipitate Identification Attempts

A number of extraction replicas have been examined using electron diffraction in an attempt to identify the precipitate. Electron diffraction has also been used on the precipitate while in the GaAs matrix. Varying sizes of diffraction apertures have been tried and exposure times as long as ten minutes used in an effort to obtain diffraction spots generated by the precipitate but to date there has been no success in this endeavor. Samples have been prepared for use in reflection electron diffraction, which will be tried in the future.

Effects of Fabrication and Quench Conditions

Some concern existed as to whether the dislocation structure was the result of the ultrasonic cutting of the discs of GaAs for the electron microscope. A number of samples were shaped by hand grinding on SiC paper to check the differences. Observations show that the ultrasonic cutting has no effect upon the observed structure.

A series of five diffusion runs, designed to test the effect of quench rate and annealing conditions, has been completed, however, electron microscope analysis is still in progress. Preliminary results indicate that annealing at temperatures below the initial diffusion temperature has no effect upon the precipitates or dislocations. As the rate of quench is increased it appears that a minor increase in extent of precipitation and dislocation generation occurs. For heavy doping, quenching at too fast a rate leads to the formation of cracks throughout the samples, thus making electron microscope observations impossible.

Effects of Composition of Diffusion Source and the GaAs

The only Zn diffusion in which no precipitates or "misfit-like" dislocations appeared was when excess arsenic was added to the diffusion source. This is consistent with many previous investigations which indicated a retardation of dislocation damage during diffusion in GaAs when excess arsenic was added.[3,4]

GaAs which was melt doped with tellurium was also used to compare the effects of Zn diffusion with those using undoped GaAs. Thus far, no differences in the precipitate or dislocation structures have been detected. GaAs melt doped with Zn was also diffused with additional Zn from a vapor source. Before diffusion, no precipitation (and very few dislocations) was observed. A control sample annealed at 800°C for 35 hours had such a high defect density that it was impossible to thin uniformly. Further attempts will be made using shorter diffusion times.

New Techniques

A technique was developed for thinning specimens from one side only, thus allowing electron microscope examination within a few microns of the

diffusion surface. This will be used in an attempt to determine whether the dislocation damage precedes or follows the precipitation process.

Because GaP is chemically similar to GaAs, and of current industrial interest, a thinning technique was developed which, though less satisfactory than the one used for GaAs, will allow examination of precipitates formed in GaP by Zn diffusion. The samples of GaP tend to pit in a symmetric pattern during chemical thinning but it is hoped that samples preliminarily thinned in this manner can be improved by use of our newly-acquired ion thinning device.

C. FUTURE PLANS

Experimental work with Zn diffusion in GaAs will be completed and extensions of the techniques to GaP will begin. Primary emphasis will include:

(1) Further quantitative studies of the effects of diffusion time, temperature, and source on precipitation in GaAs.

(2) Electron microscope studies very near the diffusion surface to determine the steps in the precipitation process.

(3) Analysis of the large amount of qualitative data gathered thus far to develop a unified explanation of the precipitation process.

(4) Further attempts at precipitate composition analysis, primarily by electron diffraction.

(5) Preliminary tests of our predictions gained from the study of GaAs applied to Zn diffusion in GaP.

REFERENCES

IV-1. G. H. Schwuttke and H. Rupprecht, J. Appl. Phys. 37, 167 (1966).

IV-2. D. B. Holt, J. Phys. Chem. Solids 27, 1053 (1966).

IV-3. J. F. Black and E. D. Jungbluth, J. Electrochem. Soc. 114, 181 (1967).

IV-4. M. Maruyama, Japan J. Appl. Phys. 7, 476 (1968).

FIGURE CAPTIONS

Figure IV-1. Multi-faceted polyhedra precipitates.

Figure IV-2. Precipitates with radially symmetric strain fields.

Figure IV-3. Precipitates with radially symmetric strain fields and faceted, strain-free precipitates.

Figure IV-4. Normal distribution of precipitates within the diffusion zone.

Figure IV-5. "Misfit-like" lines of contrast.

Figure IV-6. "Misfit-like" lines of contrast. The spots along the lines are not precipitates.

Figure IV-7. Precipitation along dislocations near the Zn diffusion front.

Figure IV-8. Precipitation along dislocations near the Zn diffusion front. Note the "misfit-like" lines of contrast in the background.

Figure IV-9. Precipitates showing distinct matrix strain contrast near the Zn diffusion front.

Figure IV-1. Multi-faceted polyhedra precipitates.

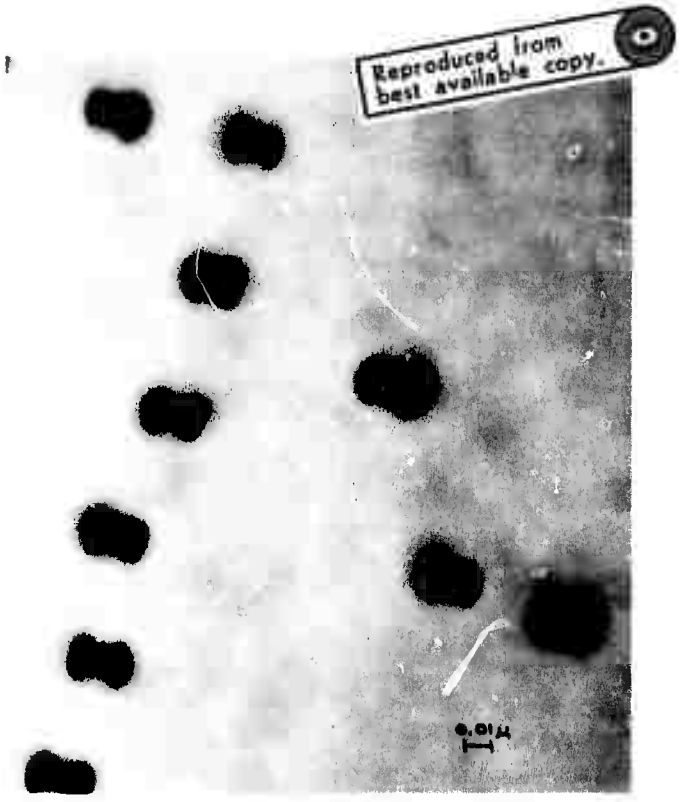

Figure IV-2. Precipitates with radially symmetric strain fields.

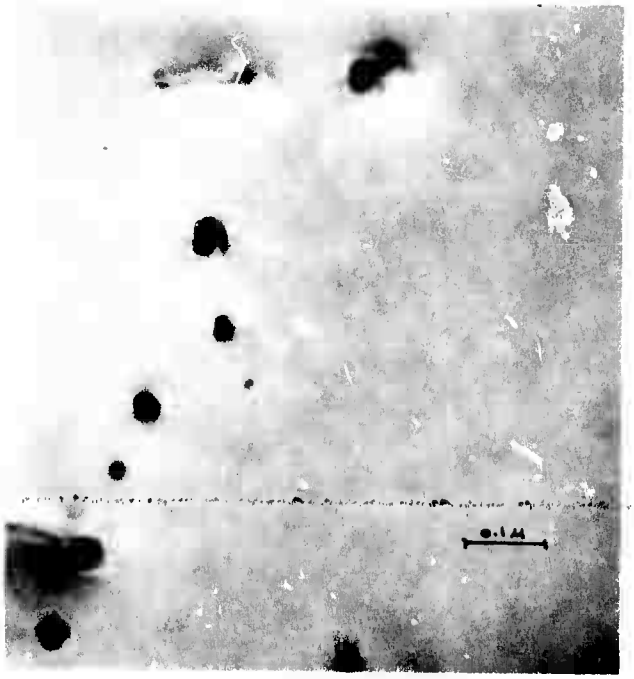

Figure IV-3. Precipitates with radially symmetric strain fields and faceted, strain-free precipitates.

Figure IV-4. Normal distribution of precipitates within the diffusion zone.

Figure IV-5. "Misfit-like" lines of contrast.

Figure IV-6. "Misfit-like" lines of contrast. The spots along the lines are not precipitates.

Figure IV-7. Precipitation along dislocations near the Zn diffusion front.

Figure IV-8. Precipitation along dislocations near the Zn diffusion front. Note the "misfit-like" lines of contrast in the background.

Figure IV-9. Precipitates showing distinct matrix strain contrast near the Zn diffusion front.

V. RELATIONS BETWEEN DISLOCATIONS AND MECHANICAL PROPERTIES AND THE PRODUCTION AND CHARACTERIZATION OF DEFECT STRUCTURES IN COMPOUND SEMICONDUCTORS

R. H. Bube, W. D. Nix, B. Liebert and A. L. Lin

A. PROGRAM OBJECTIVE

In this part of the research program we are attempting to devise techniques for modifying and characterizing the line defect structures in compound semiconductors, particularly GaAs, through high temperature mechanical deformation. The objectives of this work are to discover and understand the effects of various types of dislocations and dislocation arrays on the important electrical and opto-electronic properties of GaAs and to suggest ways of utilizing dislocations in devices. Our present work on GaAs is motivated by the extensive microwave device research on this material at Stanford. It is expected that our work will contribute to the device research and to the related crystal growing effort by providing basic information about the effect of dislocations in these crystals.

The basis for our experimental work was founded by W. T. Read[1-3] who, following the suggestion of Shockley[4], theoretically predicted that edge dislocations in elemental semiconductors should act as acceptors at sufficiently low temperatures. This aspect of Read's theory was subsequently verified by the elegant experiments of Logan, Pearson and Kleinman[5] in n-type Ge. These experiments are particularly relevant to our work as they represent one of the things we are trying to do with GaAs. Logan et al.[5] found that the introduction (by bending at high temperatures) of edge dislocations into Ge crystals containing 2×10^{14} Sb atoms cm^{-3} causes the carrier concentration to decrease at low temperatures, thereby indicating acceptor action. They also found that the Hall

mobilities measured for current flowing parallel to the dislocations are experimentally indistinguishable from the corresponding measurements on undeformed crystals. These results definitely indicate that dislocations can be introduced into Ge crystals in such a way that the carrier concentration is reduced while the Hall mobility remains unchanged. One of our objectives is to determine if the same effects can be produced in GaAs. Evidently such effects could be used in devices if they could be properly controlled.

This research effort is being carried out on two types of GaAs: nominally pure GaAs with low carrier density, similar to the material used for active films in the microwave devices, and high resistivity Cr doped material, similar to the insulating substrates used for the LPE growth of active layers. A discussion of research progress on each of these materials is given below.

B. PROGRESS: PURE GaAs

Our experimental work to date has been performed on nominally pure n-type GaAs crystals with carrier concentrations of 3.0×10^{16} cm^{-3}. We have introduced edge dislocations (both α and β^*) to a density of about 2×10^{7} cm^{-2} and have measured the carrier concentration and Hall mobility as a function of temperature from 77°K to 330°K. The experimental procedures and the results of this work are given in the following paragraphs.

Experimental Procedure

Crystals of bulk grown n-type GaAs obtained from Bell and Howell with carrier concentration of about 3×10^{16} cm^{-3} and room temperature

---

* α and β dislocations refer to edge dislocations for which the "extra half plane" terminates with gallium and arsenic atoms respectively.

mobilities about 5000 cm^2/V-sec were cut into 2x2x25 mm samples with a high speed diamond saw. The orientation of these samples is shown in the illustration below and was chosen so that both active {111} slip planes are symmetrically located forming angles of 55° with the direction of maximum shear.

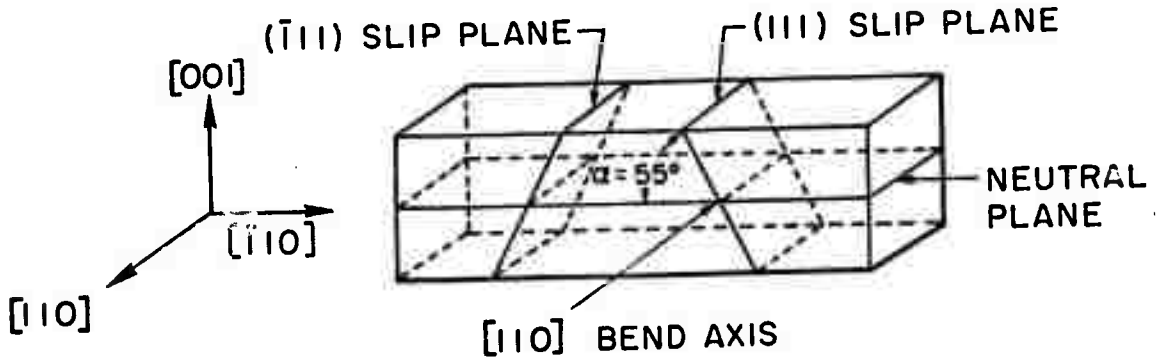

The surfaces of these samples were cleaned and then chemically polished. Cleaning, for the purpose of removing oil contamination introduced during cutting and handling, was accomplished by boiling for 10 minutes each in trichloroethylene and acetone, rinsing first in de-ionized water and then in methanol. The cleaned samples were then etched for 1 minute in 3 parts H_2SO_4, 1 part H_2O_2 (31%), and 1 part H_2O heated to 65°C.

A new method for obtaining contacts that remained ohmic at temperatures down to 77°K was discovered. Indium metal was added to a small amount of mercury until no more would be dissolved. The resulting amalgam was applied to the [110] faces with an artist's brush and heated in a hydrogen atmosphere for 1 minute at 400°C. This method offers several advantages over more conventional techniques. No special masks or evaporating apparatus is necessary to obtain very narrow contacts. The total time required to apply all contacts necessary for a Hall measurement is less than 10 minutes. The short time the samples are actually at temperature (about 1 minute) does not cause deletorious effects (GaAs is known

to convert from n to p-type after heat treatment[6,7]). Finally, the contacts are easily removed by washing in a warm HCl solution for a few minutes.

The Hall constant, mobility and resistivity were measured for each sample both before and after deformation (normal to the induced dislocations). The Hall apparatus consisted of a Dewar, an electrically heated sample holder with 6 leads, a copper-constantan thermocouple positioned near the sample, and an electromagnet. Magnetic fields up to 4000 gauss were used. A current of 10 ma was supplied with a constant current power source and measured by the voltage drop across a 0.1% precision 1 ohm resistor. All voltages were measured with a Leeds and Northrup type K-2 potentiometer.

After cooling to LN temperature (77°K) in a helium atmosphere, electrical measurements were made and then, by adjustment of the sample heater, steady state temperatures up to 330°K were maintained.

To prepare the samples for bending the old contacts were removed and new ones applied to the underside of the crystal at the ends in order to achieve an electrical contact with the graphite electrodes. Three samples were chosen for each bending experiment. Two of these samples were properly oriented (by etching the {111} planes) to yield an excess of either alpha (Ga) or beta (As) dislocations when subsequently bent. The other sample was used as a control (i.e., only heated, not bent). The samples were heated by direct current (10A at 15V) and bending carried out at 550°C in an argon atmosphere using the apparatus described in the previous progress report.

It was necessary to heat all three samples slowly to prevent localized hot spots from occurring and then to allow the temperature to

equilibrate throughout before bending. All samples were bent to a 2 cm radius of curvature corresponding to 2×10^7 dislocations/cm^2.

On reaching the required amount of bending (determined by an external mechanical stop) the current was switched off allowing the samples to cool to room temperature. The whole process of heating, bending, and cooling took 2-3 minutes. After bending, the samples were cleaned and then chemically polished, as before, in order to remove any damaged surface layer.

Experimental Results

The principal experimental results are shown in the Figures V-1 and V-2. Even though the samples were at temperature only a short time and the surface was subsequently removed by etching, a reduction in both mobility (about 12%) and carrier concentration (about 30%) occurred for the control sample (for measurements at 77°K).

The net effect of the bending causes an increase in carrier density for both the alpha and beta bent samples of 18% and 26% respectively. The alpha bent sample showed no change in mobility while the mobility in the beta bent sample was reduced by 8% compared to the control.

With a dislocation density of 2×10^7 cm^{-3}, the total number of dislocation centers is <u>at most</u> $2 \times 10^7/b = 5 \times 10^{14}$ cm^{-3}, where b is the Burger's vector (4×10^{-8} cm for GaAs). When Coulomb repulsion is taken into account, then even when f (the fraction of <u>occupied</u> dislocation sites) = 0.1, the number of effective donor or acceptor centers provided by dislocations cannot exceed 5×10^{13} cm^{-3}. The existing carrier concentration, 3×10^{16}, should be sufficiently high to mask any effect of the bending. However, we do see significant changes in carrier concentration and mobility. These effects are very large and difficult to explain with the usual application of Read's theory[1-3]. We plan to extend our present measurements

to 4°K in an effort to identify the important scattering mechanisms. This will help us to explain the anomalously large effects reported here.

It has also been observed in some bent samples that there is a significant inhomogeneity in resistivity. It is found (see diagram below) that $\rho_{12}<\rho_{34}<\rho_{56}$.

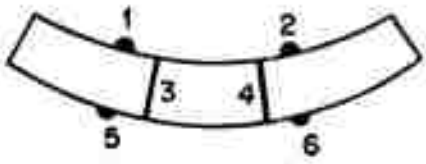

These variations in resistivity tend to diminish as one proceeds from the surface into the interior.

It is possible that these variations in resistivity are due to differing point defect concentrations in these regions. The concave surface is under a considerable compressive stress which should tend to favor the formation of interstitial defects. Since interstitial gallium atoms are known to act as donors[8] they would reduce the resistivity near the concave surface if they were present. However, the convex surface experiences a tensile stress which could very likely result in a stress-enhanced evaporation of arsenic from the surface. Acceptor behavior is suspected for arsenic vacancies[7,9] which would result in a decrease in carrier concentration and an increase in resistivity. It is interesting to note that the value of the resistivity for the flat face is between the other two values.

C. FUTURE WORK: PURE GaAs

One of the deficiencies of the experimental work performed to date is that the carrier concentration is larger than the density of dislocation sites introduced by bending. This defect exists in all but one previous

study of the effects of dislocations on the electrical properties of semiconductors[10-12]. It is not practical to introduce dislocation densities higher than about 2×10^7 cm^{-2}. Therefore it is necessary to obtain crystals with lower carrier concentrations. Until recently this has not been possible. However, the Crystal Growing Group has shown that epi-layers of GaAs with low 10^{14} cm^{-3} carrier concentrations, can be grown onto semi-insulating GaAs substrates. These concentrations are lower than the dislocation site concentrations which can be introduced by bending. It is proposed to investigate the effects of dislocations on the properties of these epi-layers by bending the crystals at high temperatures in the usual way. One special problem with these samples (which we have solved) is that only the epi-layer is conducting and that it must act as a heater for the entire sample composite during high temperature bending. It is anticipated that these experiments will show effects similar to those found in Ge by Logan et al.[5]

If the introduction of dislocations into epi-layers of GaAs has large effects on the electrical properties, as we expect, subsequent work will be directed toward controlling the density type (edge or screw) and arrangement of dislocations in deformed crystals and studying the effects of these variables on the electrical properties.

D. PROGRESS: HIGH RESISTIVITY GaAs:Cr

Properties of GaAs:Cr

Since Cronin and Haisty[13] announced in 1964 the possibility of preparing high-resistivity GaAs consistently by the incorporation of Cr impurity, a number of investigations of the properties and associated energy levels of this impurity have been carried out.[14-19] Measurements

of photoconductivity as a function of wavelength and temperature, of optical absorption, of optical quenching of photoconductivity, of Hall coefficient in the dark as a function of temperature, and of photoluminescence emission, have contributed to a growing model for the properties of GaAs:Cr. Data available prior to the beginning of our investigation in this program indicated that at least two levels were involved with the energy levels indicated in Figure V-3. It has been uncertain whether both levels A and B should be attributed to the Cr impurity, but they appear to be present in all samples of GaAs:Cr prepared to date, including our own data to be described below.

Maxima in the photoconductivity response spectrum correspond to intrinsic excitation near the band edge and to extrinsic excitation from Level A to the conduction band. Between these two maxima, a deep minimum in photoconductivity is found at low temperatures, associated with optical quenching of photoconductivity due to excitation of electrons from the valence band to Level B.

It is this delicately balanced, photoelectronically active impurity situation in GaAs:Cr which we are using as the matrix for detection of effects due to heating without deformation, and to heating with bending deformation.

Previous Work on Deformation of GaAs

Kravchenko et al.[12] investigated the effect on Hall coefficient and mobility of deforming n-type GaAs crystals with electron densities in the range of 1.8×10^{16} to 3×10^{17} cm^{-3}. Deformation was at temperatures between 500° and 720°C, in vacuum, about the [110] axis, and to a 7-cm radius of curvature. Deformation and short-duration heat treatment at 500°C

resulted in a slight decrease in electron density and mobility. Effects of deformation at higher temperatures (650° - 720°C) divided the samples into two groups: (1) in what were presumably purer samples, deformation increased the electron density and the electron mobility; (2) in what were presumably relatively impure compensated samples, deformation and heat treatment decreased the electron density and increased the electron mobility. For samples of type (1), heating alone produced changes in the same direction as deformation, but of smaller magnitude. Effects of type (1) were explained in terms of impurity (copper acceptors) diffusion to dislocations followed by precipitation; effects of type (2) were explained in terms of copper diffusing from the surface and formation of arsenic vacancies.

Two papers treating the determination of the density of dislocations induced by deformation of GaAs are also relevant to our work. According to S. P. Grishina et al.[20] the etch pits revealed on the (111) surface by suitable etching correspond to the outcrops of dislocations, and there is a one-to-one relationship between the dislocation density in the crystal and the etch-pit density on the (111) planes. On the other hand, Malikova et al.[21] investigated the density of dislocations revealed by etching on the (111) surface and found an order-of-magnitude distribution of dislocation density over the cross section of the deformed GaAs sample, the density in the center being almost ten times smaller than the density at the faces of the crystal. Annealing at 1100°C for 50 hours after deformation resulted in equalization of the dislocation density across the cross section of the sample to within about 20 percent at an intermediate density.

Experimental Procedure

Two rectangular GaAs:Cr single crystal samples (25 x 2 x 2 mm^3) from the same ingot and with the same dark conductivity (5 x 10^{-9} ohm^{-1} cm^{-1})

were selected. The upper face of the bar was parallel to the (100) plane, and the side and front faces were parallel to the (110) plane. The average etch-pit density on the (111) plane of these two samples was 9.2×10^4 cm^{-2}. To reveal the etch-pit density on the A surface (111), Shell's etchant was used (1 part HNO_3 + 2 parts H_2O) or Richards-Crocker etchant (1 part HF + 7 parts HNO_3 + 12 parts H_2O + 1 percent molar solution of $AgNO_3$). The latter solution also produced etch pits on the B surface ($\overline{111}$). Before etching, each surface was lapped with 7 micron SiC powder, mechanically polished with 0.3 micron Linde A aluminum abrasive, and chemically polished in a solution of H_2SO_4:H_2O_2:H_2O = 3:1:1 (or a 5:100 solution of bromine in methanol). Figure V-4 shows one of the results of etching.

One of the samples was cut in half, one half of which was retained as the as-grown sample, and the other half of which was used as a control sample for the effects of heating without deformation. The long bar left was bent under argon atmosphere with a 1.2 Kg load at 580°C for 50 min in a 4-point quartz bending apparatus to produce α-dislocations, after a 10 min preheating period. The control sample was placed adjacent to the bending sample. In the data given below, we refer to the as-grown sample as A, the control sample as H, and the deformed sample as D.

After bending, a face about 0.5 cm from the end of the sample was ground at an angle of 55° to the upper face to obtain the (111) surface. Figure V-5 shows the results of etching on this surface. The neutral line is seen quite sharply. The average etch pit density near the surface in Figure V-5 was found to be equal to 1.1×10^7 cm^{-2} as determined from X2000 pictures obtained with a scanning electron microscope. The theoretical dislocation density was calculated from Nye's formula:

$$\rho = \frac{1}{R\, b \cos \theta}$$

where $b \cos \theta = 2 \times 10^{-8}$ cm for the bending orientation chosen, and $R = 3.2$ cm near the middle of the bent sample. Thus the calculated value for the dislocation density ρ is 1.6×10^{7} cm^{-2}.

For electrical measurements, a sample ($8.3 \times 2 \times 2$ mm^3) was cut from the center of the deformed bar. A thickness of about 150 microns total was removed from the faces of the control sample and the bent sample by mechanical and chemical polishing to remove possible surface effects. After cleaning all three samples, 6-point indium contacts suitable for Hall measurements were made by alloying under H_2 at 375°C for 5 min.

Experimental Results

Hall effect vs. photon energy spectral response of photoconductivity results are given in Figure V-6 for measurements at 294°K. Structure in the spectral response corresponds to intrinsic excitation across the band gap of GaAs corresponding to the maximum at 1.43 eV, and extrinsic maxima at 1.11 eV and 0.9 eV, with a low-energy threshold of about 0.65 eV. The variation of the mobility with wavelength suggests that hole excitation may be involved at the 1.1 eV band. Heating uniformly decreases the electron lifetime equally at all wavelengths by 40 percent; with the control sample as reference, bending decreases the electron lifetime for strongly absorbed light (excitation near the surface) by 80 percent, and for extrinsic excitation by between 15 and 50 percent. Heating increases the electron mobility by 10 to 30 percent; with the control sample as reference, bending decreases the electron mobility by 50 to 80 percent. A summary of the effects of heating and bending is given in Table V-I for ease of reference.

The spectral dependence of $(1/R_H e)$ at 83°K is shown in Figure V-7. At this temperature there are strong two-carrier effects. In the as-grown A sample, there is a large dip in photoconductivity between 1.0 and 1.3 eV; in the control sample H, the conductivity in this spectral range is actually dominated by holes. Measurements for the deformed sample in this spectral range have not been completed and are missing from Figure V-7. Measurements between 1.0 and 1.5 eV are very time-consuming to make; times of the order of 5 to 10 hr often being required to reach steady state following photo-excitation previously at either lower or higher energies.

Structure in these low-temperature spectral response curves consists of the intrinsic maximum at 1.43 - 1.48 eV (with rapid decrease in electron lifetime for higher energies and strongly absorbed light), the extrinsic maximum at 0.87 eV, small structure at 0.78 eV, and a low-energy threshold at about 0.7 eV. The effect of heating is to decrease both the intrinsic and extrinsic response by about 85 percent; with the control sample as reference, the effect of deformation is to increase both the intrinsic and extrinsic response by about 35 percent.

The mobility data corresponding to Figure V-7 are given in Figure V-8. Although there are some apparent differences in structure between the curves obtained for the different samples, the main features are identifiable. For energies greater than 1.6 eV in the intrinsic region, true one-carrier electron photoconductivity is indicated; in the range of the 0.87 eV extrinsic maximum, however, two-carrier effects are still strong. All samples show a minimum at about 0.80 eV followed by a maximum at about 0.9 eV. Minima in Figure V-8 can be interpreted as indicating increased density of free holes; hence correlation of the small maximum at 0.78 eV in Figure V-7 with the minimum at 0.8 eV in Figure V-8 suggests that this

peak is due to hole excitation. The effect of heating is to leave unchanged the mobility in the truly intrinsic range for photon energies above 1.6 eV (although some effect near the edge at about 1.5 eV is indicated), and to decrease the Hall mobility in the extrinsic maximum by 60 percent. With the control sample as reference, the effect of deformation is to decrease the Hall mobility in the intrinsic range by 80 percent and to increase the Hall mobility in the extrinsic range by 20 percent.

The dependence of the optical quenching of photoconductivity, responsible for the behavior in the 1.0 - 1.3 eV range of Figures V-7 and V-8, on the photon energy for quenching can be measured directly. The sample is excited with an intrinsic primary light, and a secondary quenching light is shined on the sample simultaneously. The reduction in the primary-excited current because of the secondary quenching radiation can then be expressed as percent quenching, as indicated in Figure V-9. The region of active quenching extends from 0.9 to 1.4 eV, with a subsidiary quenching maximum at 0.8 eV for the heated sample at 80°K. Quenching spectra for the deformed sample still need to be obtained.

In order to determine the variation of lifetime and mobility with temperature, measurements of photoconductivity and photo-Hall effect were made as a function of temperature for photoexcitation at the maxima of the response spectra at low temperatures for both intrinsic and extrinsic photoexcitation. The data shown in Figure V-10 are for intrinsic excitation and in Figure V-11 for extrinsic excitation. The dark data included in Figures V-10 and V-11 show that the dark value of $(1/R_H e)$ is not affected by either heating and deformation. The result suggests that the levels affected by heating and deformation lie above the dark Fermi level. Because of the small temperature range available for dark measurements, an accurate

measurement of the dark activation energy is not possible. The as-grown and control sample have an activation energy for $(1/R_H e)$ of 0.13 eV in the high-temperature range, and all three samples have an activation energy of -0.06 eV in the low-temperature range, for intrinsic excitation. The apparent discrepancy between the mobility data of Figure V-10 and Figure V-8 is removed when it is realized that the photon energy used for the "intrinsic" data of Figure V-10 was 1.45 eV. For extrinsic radiation, all samples again have an activation energy over the intermediate and low temperature range of -0.06 to -0.07 eV.

Discussion of Results

It is evident from the above set of data that a detailed discussion of the results requires a fairly detailed model of the energy level structure in GaAs:Cr which is consistent with a major portion of the observed effects. The simple model of Figure V-3 is still partially adequate, but it is clear that more than two levels are required to account for the rich variety of the experimental results. Derivation of a suitable model, capable of giving the basic photoconductivity characteristics observed, will then permit interpretation of the effects of heating and deformation in terms of variations in imperfection densities and levels.

Some of the levels detected as structure in the photoconductivity spectra may not of course be associated with the Cr impurity. Certain similarities may be noticed in previously reported data on heat-treated GaAs crystals[22] or GaAs:O crystals.[23] An activation energy of -0.07 eV was reported for $(1/R_H e)$ under photoexcitation in "pure" crystals of GaAs with 300°K-conductivity of 10^{-8} ohm^{-1} cm^{-1};[24] if correction is made for the temperature dependence of density of states, a value of -0.09 eV for the activation energy is obtained.

The effect of heating in argon for 60 min at 580°C is to decrease the electron lifetime at all temperatures, but more at low temperatures than at room temperature. Where one-carrier effects dominate at 300°K, the effect of heating is to slightly increase the electron mobility. At low temperatures, where two-carrier effects dominate, heating accentuates the contribution of holes to the photoconductivity and the effects of optical quenching of photoconductivity. The observed decrease in Hall mobility for extrinsic photoexcitation at 80°K can be associated with this effect.

The effect of deformation at 580°C to a radius of curvature of 3.2 cm can be expressed with reference to the state of the control sample subjected to a similar heating without deformation. Deformation decreases the electron lifetime at room temperature, more for strongly absorbed (surface absorbed) light than for extrinsic (volume absorbed) light, as might be expected from the higher concentration of dislocations near the surface. Deformation appears to counteract the tendency of heating alone to accentuate two-carrier effects at low temperature, although the data here are not complete at the present time. Thus the increase in $(1/R_H e)$ at 80°K produced by deformation can be considered as a reduction in the hole contribution to the Hall coefficient. Deformation also decreases the Hall mobility at 300°K, an effect which is even stronger for intrinsic photoexcitation at 80°K. The increase in Hall mobility for extrinsic excitation caused by deformation can again be identified with a decrease in participation by free holes as a result of deformation.

The fact that the dark value of $(1/R_H e)$ at 300°K is not changed by either heating or deformation is consistent with the control of equilibrium conditions by the density of imperfections in the as-grown crystals, only

minor perturbations in these densities being caused by heating or deformation. Heating also produces no change in the dark value of the Hall mobility at 300°K, but additional scattering associated with the dislocations does produce a slight decrease in the dark mobility.

E. FUTURE WORK: HIGH RESISTIVITY GaAs:Cr

1. Construction of a suitable model and interpretation of the data in more detail in terms of that model.

2. Completion of the unfinished data indicated above for the deformed sample.

3. Deform to produce β-dislocations to compare with α-dislocations.

4. Produce deformation to different radii of curvature to correlate effects with dislocation density.

5. Anneal samples after deformation to see effects on photoelectronic properties measured subsequently.

6. Investigate the possibility of starting with GaAs:Cr material with lower initial dislocation density, to intensify the changes observed.

The results given here show that we have been successful in demonstrating that both heating and deformation by bending produce easily measurable order-of-magnitude effects in the photoelectronic properties of GaAs:Cr. The value of this part of the program extends, therefore, beyond the direct determination of the effects of mechanical deformation by bending, to include effects of heat treatment and basic information about the electronic phenomena occurring in high-resistivity GaAs.

REFERENCES

V-1. W. T. Read Jr., Phil. Mag., 45, 775 (1954).

V-2. W. T. Read Jr., Phil. Mag., 45, 1119 (1954).

V-3. W. T. Read Jr., Phil. Mag., 46, 111 (1955).

V-4. W. Shockley, Phys. Rev., 91, 228 (1953).

V-5. R. A. Logan, G. L. Pearson and D. A. Kleinman, J. Appl. Phys., 30, 885 (1959).

V-6. E. Muñoz, W. L. Snyder and J. L. Moll, Appl. Phys. Lett., 16, 262 (1970).

V-7. Masaharu Toyama, Japan. J. Appl. Phys., 8, 1000 (1969).

V-8. F. A. Kroger, The Chemistry of Compound Semiconductors, from the book, "Physical Chemistry - an Advanced Treatise", Wilhelm Jost Ed. (1970).

V-9. H. R. Potts and G. L. Pearson, J. Appl. Phys., 37, 2098 (1966).

V-10. H. Alexander and P. Haasen, Solid State Physics, 22, 146 (1968).

V-11. W. Schröter, Phys. Stat. Sol., 21, 211 (1967).

V-12. A. F. Kravchenko, A. M. Palkin and V. P. Ruleva, Sov. Phys.-Semiconductors, 1, 922 (1968).

V-13. G. R. Cronin and R. W. Haisty, J. Electrochem. Soc., 111, 874 (1964).

V-14. R. F. Broom, J. Appl. Phys. 38, 3483 (1967).

V-15. D. R. Heath, P. R. Selway and C. C. Tooke, Brit. J. Appl. Phys. Ser. 2, 1, 29 (1968).

V-16. G. A. Allen, Brit. J. Appl. Phys. Ser. 2, 1, 593 (1968).

V-17. N. M. Kolchanova, D. N. Nasledov, M. A. Mirdzhalilova, and V. Yu. Ibragimov, Sov. Phys.-Semiconductors 4, 294 (1970).

V-18. O. V. Tretyak, Sov. Phys.-Semiconductors 4, 517 (1970).

V-19. E. M. Omelianovski, Bull. Am. Phys. Soc. 15, 1615 (1970).

V-20. S. P. Grishina, M. G. Mil'vidskii, and V. B. Osvenskii, Inorg. Mat., trans. from Izv. ANSSSR Neorganiche Materialy, 2, 1549 (1966).

V-21. E. A. Malikova, R. L. Petrusevich, and E. S. Sollertinskaya, Sov. Phys.-Crystallography 11, No. 6, 760 (1967).

V-22. J. Blanc, R. H. Bube, and L. R. Weisberg, J. Phys. Chem. Solids 25, 225 (1964).

V-23. E. Omelianovski and R. H. Bube, J. Appl. Phys. to be published.

V-24. R. H. Bube and H. E. MacDonald, Phys. Rev. 128, 2062 (1962).

TABLE V-I

SUMMARY OF EFFECTS OF HEATING AND DEFORMATION (α-DISLOCATIONS) ON GaAs:Cr

		$(1/R_H e)$		μ_H	
		Intrinsic*	Extrinsic*	Intrinsic*	Extrinsic*
Heating (60 min, 580°C Argon)	300°K	Decrease 40%	Decrease 40%	Increase 10-30%	Increase 10-30%
	80°K	Decrease 85%	Decrease 85%	No change	Decrease 60%
Deformation** (R = 3.2 cm)	300°K	Decrease 80%	Decrease 15-50%	Decrease 50%	Decrease 40-80%
	80°K	Increase 35%	Increase 35%	Decrease 80%	Increase 20%

* The terms "intrinsic" and "extrinsic" refer to the spectral range of the photoexcitation being used. Dark $(1/R_H e)$ near 300°K is not changed either by heating or by deformation. Dark μ_H near 300°K is not changed by heating (2200 cm^2/V-sec), and is decreased by about 20 percent by deformation.

** The results cited as due to deformation are stated with the state caused by heating as the reference.

Figure Captions

Figure V-1 Temperature dependence of the electron concentration in n-type GaAs before and after plastic bending at 550°C.

Figure V-2 Temperature dependence of the electron mobility of n-type GaAs before and after plastic bending at 550°C.

Figure V-3 Energy level scheme for Cr impurity in GaAs from previous investigations.

Figure V-4 Etch pits revealed on the B surface after etching in Richards-Crocker solution for 8 minutes at 35°C, x200.

Figure V-5 Etch pits revealed on the A surface of the deformed sample (about 0.5 cm from the end of the sample), x50.

Figure V-6 Spectral variation at 300°K of the reciprocal Hall coefficient and the Hall mobility for the (A) as-grown sample, (H) heat-treated control sample, and (D) deformed sample.

Figure V-7 Spectral variation at 80°K of the reciprocal Hall coefficient for the (A) as-grown sample, (H) heat-treated control sample, and (D) deformed sample.

Figure V-8 Spectral variation at 80°K for the Hall mobility for the (A) as-grown sample, (H) heat-treated control sample, and (D) deformed sample.

Figure V-9 Spectral variation of optical quenching efficiency at 80° and 300°K for the (A) as-grown sample, and (H) heat-treated control sample.

Figure V-10 Temperature dependence of the reciprocal Hall coefficient in the dark, and of the reciprocal Hall coefficient (solid curves) and of the Hall mobility (dashed curves) for intrinsic photoexcitation for the (A) as-grown sample, (H) heat-treated control sample, and (D) deformed sample.

Figure V-11 Temperature dependence of the reciprocal Hall coefficient in the dark, and of the reciprocal Hall coefficient (solid curves) and of the Hall mobility (dashed curves) for extrinsic photoexcitation for the (a) as-grown sample, (H) heat-treated control sample, and (D) deformed sample.

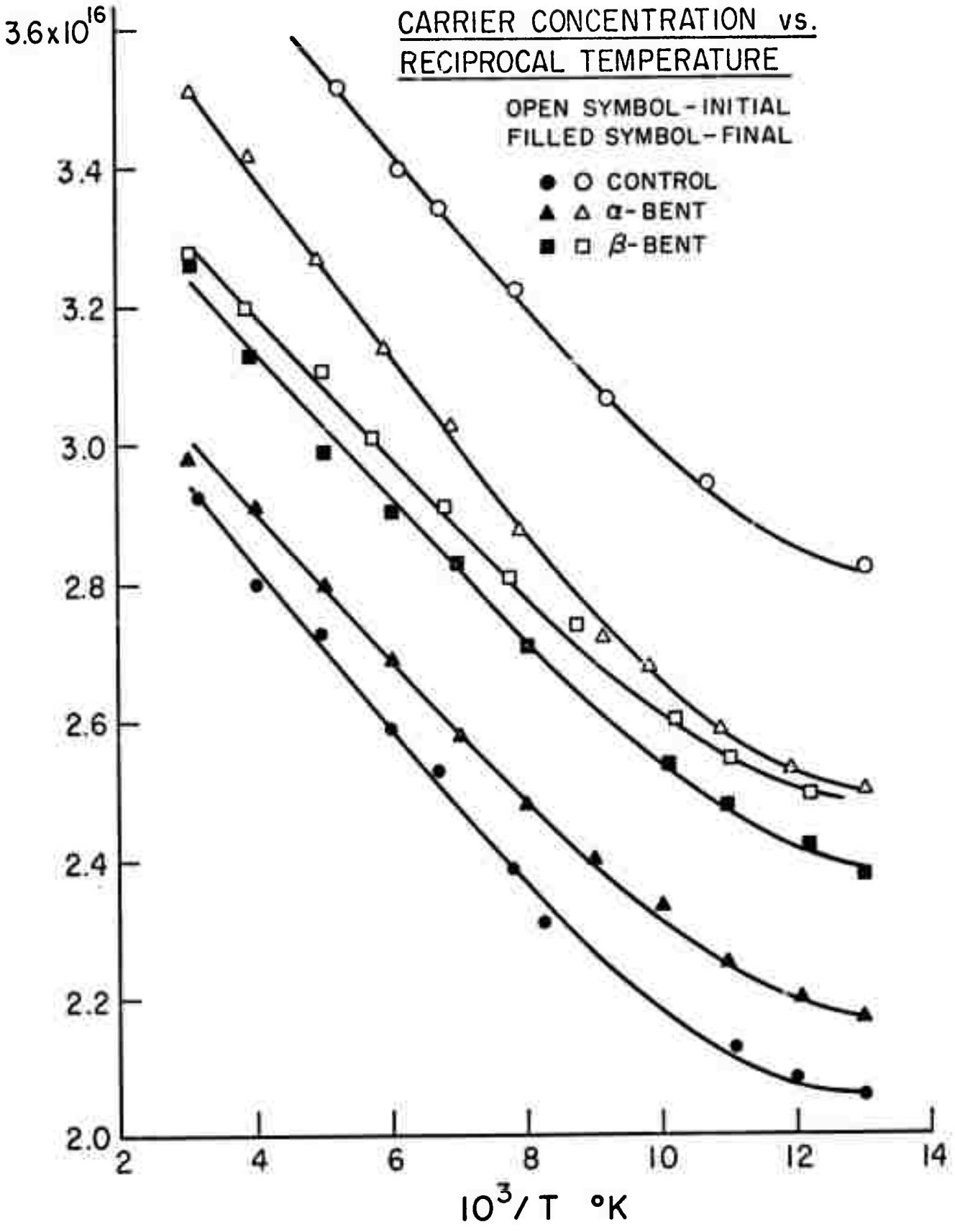

Figure V-1. Temperature dependence of the electron concentration in n-type GaAs before and after plastic bending at 550°C.

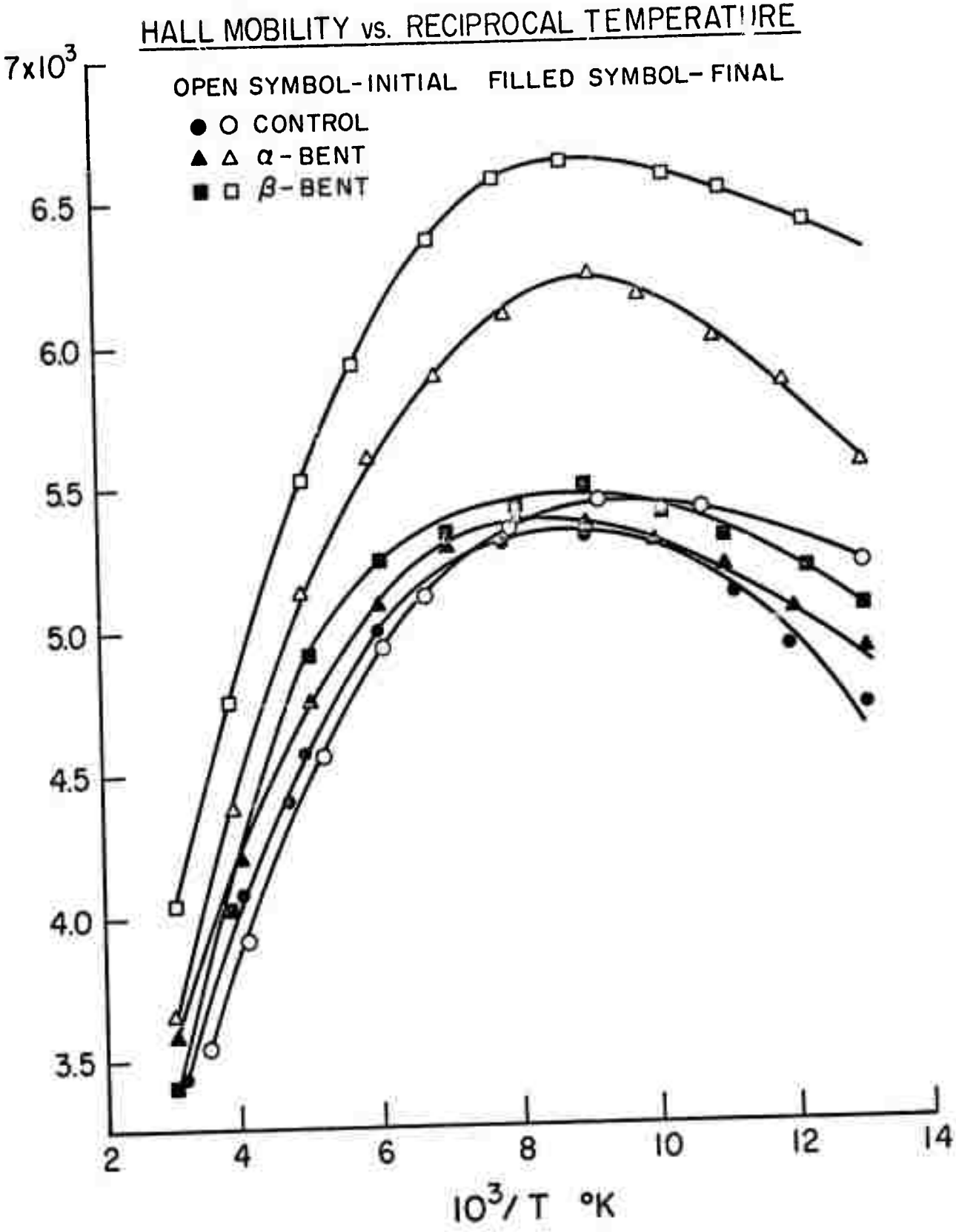

Figure V-2. Temeprature dependence of the electron mobility of n-type GaAs before and after plastic bending at 550°C.

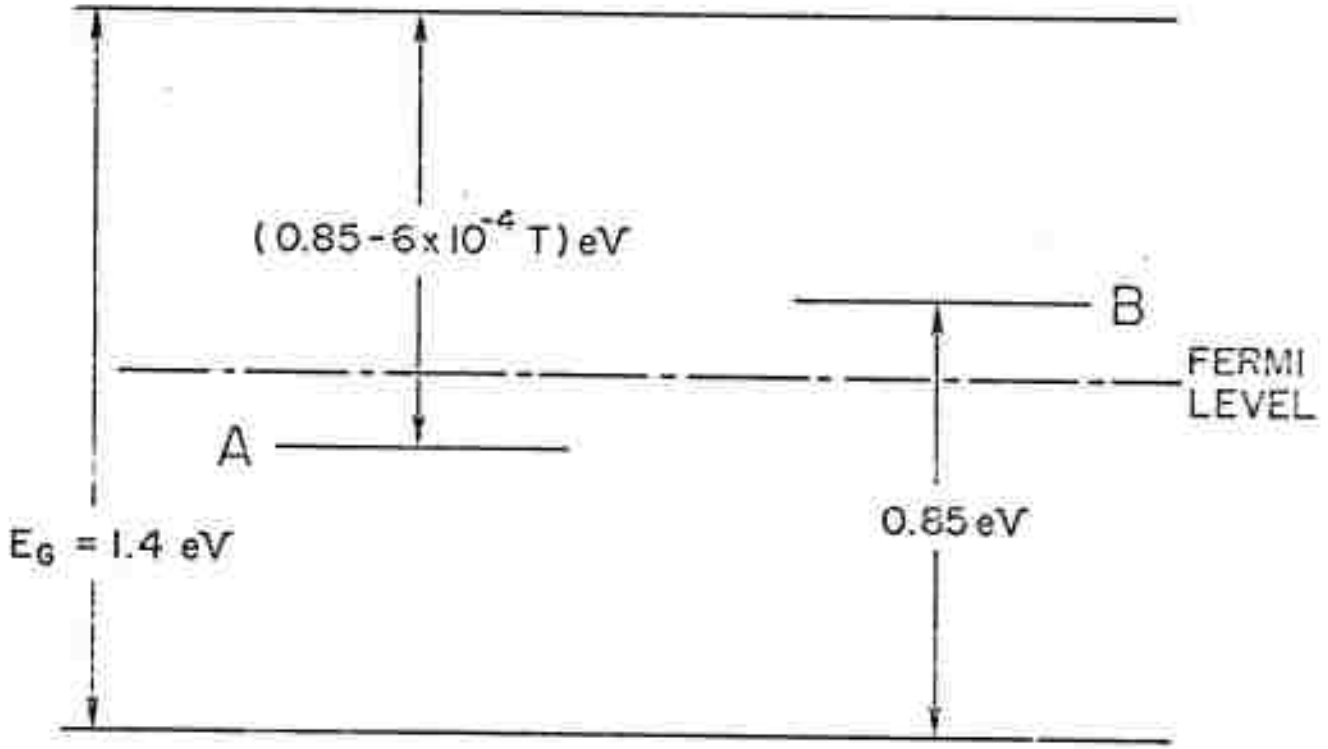

Figure V-3. Energy level scheme for Cr impurity in GaAs from previous investigations.

Figure V-4. Etch pits revealed on the B surface after etching in Richards-Crocker solution for 8 min at 35°C, x200.

Figure V-5. Etch pits revealed on the A surface of the deformed sample (about 0.5 cm from the end of the sample), x 50.

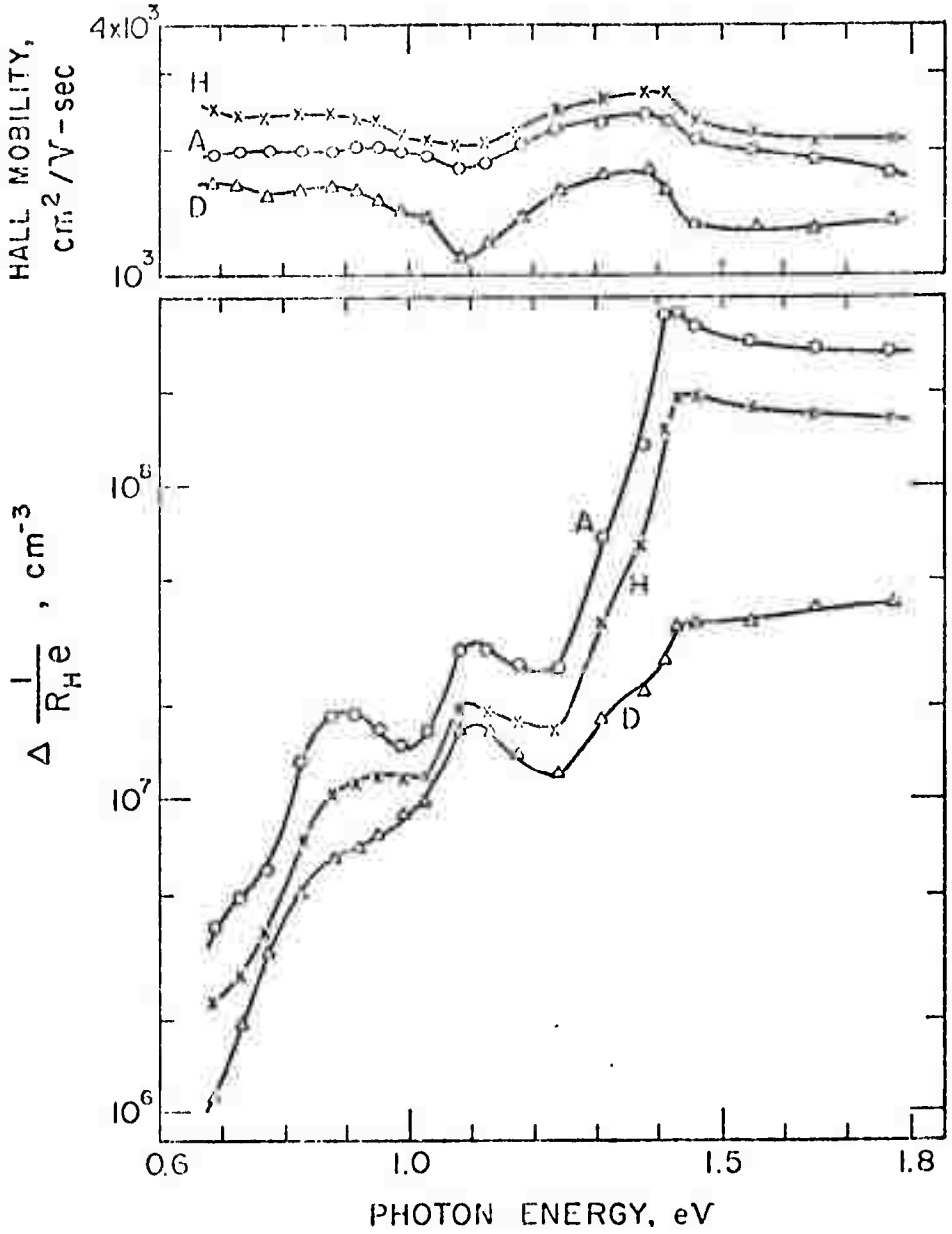

Figure V-6. Spectral variation at 300°K of the reciprocal Hall coefficient and the Hall mobility for the (A) as-grown sample, (H) heat-treated control sample, and (D) deformed sample.

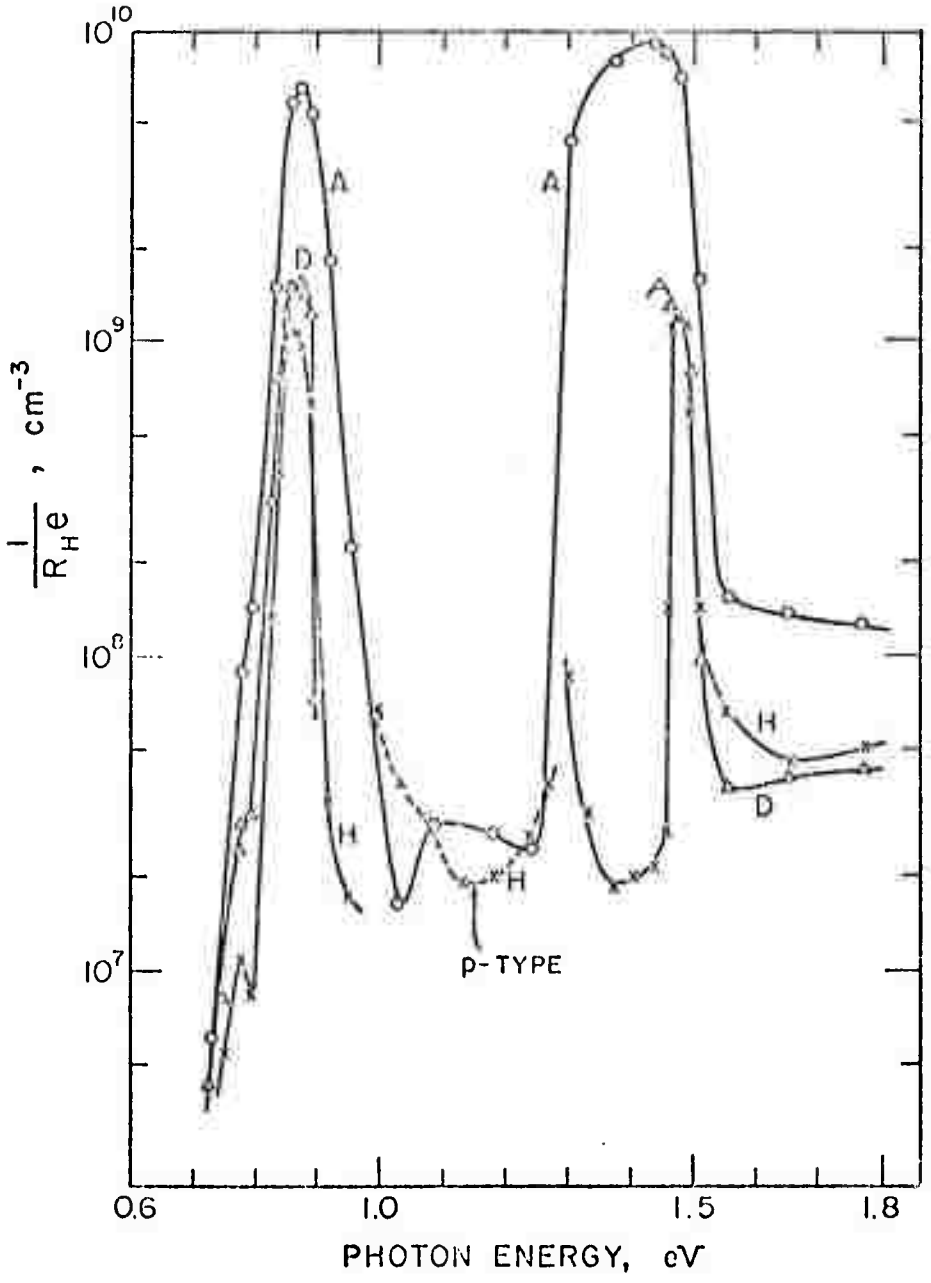

Figure V-7. Spectral variation at 80°K of the reciprocal Hall coefficient for the (A) as-grown sample, (H) heat-treated control sample, and (D) deformed sample.

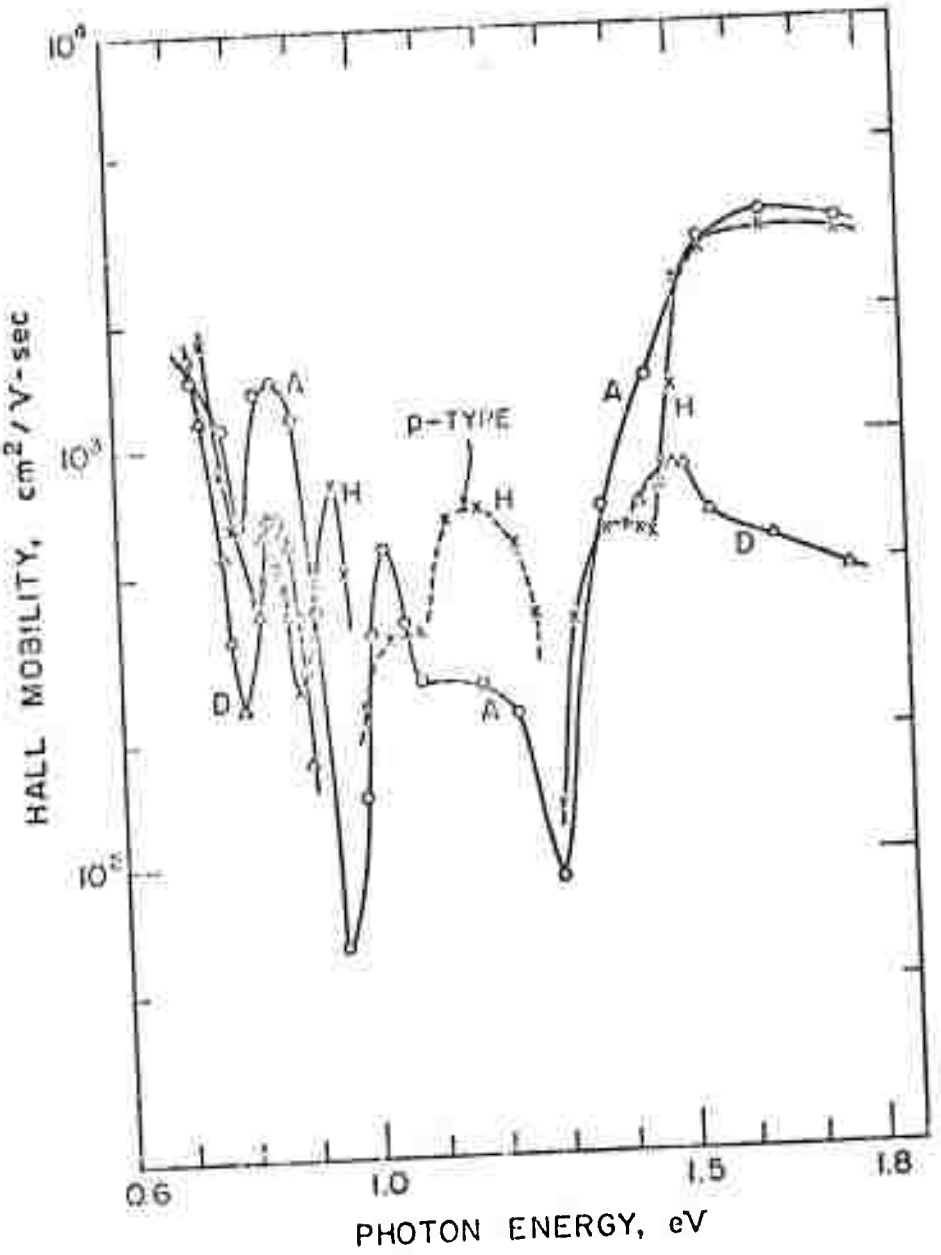

Figure V-8. Spectral variation at 80°K for the Hall mobility for the (A) as-grown sample, (H) heat-treated control sample, and (D) deformed sample.

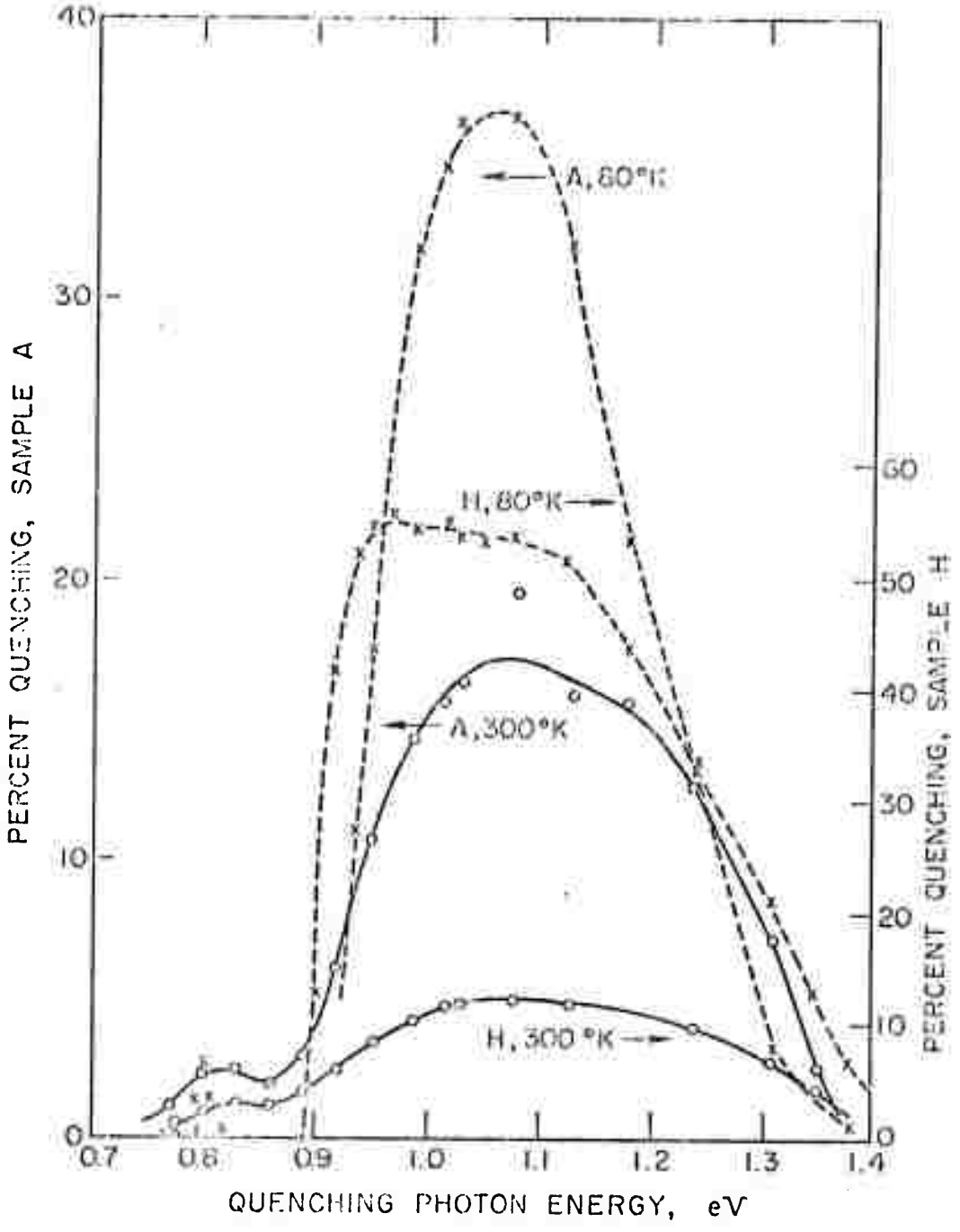

Figure V-9. Spectral variation of optical quenching efficiency at 80° and 300°K for the (A) as-grown sample, and (H) heat-treated control sample.

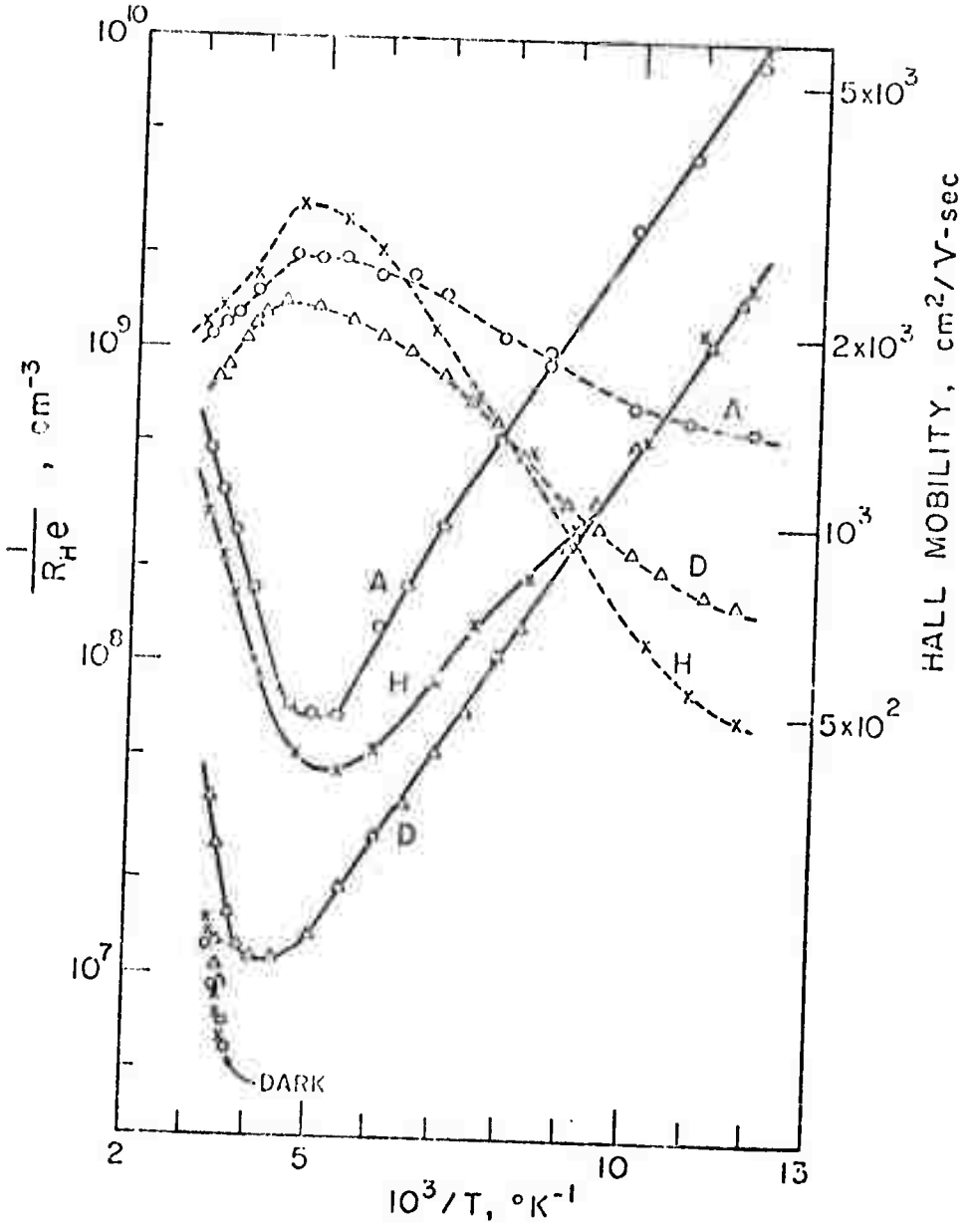

Figure V-10. Temperature dependence of the reciprocal Hall coefficient in the dark, and of the reciprocal Hall coefficient (solid curves) and of the Hall mobility (dashed curves) for intrinsic photoexcitation for the (A) as-grown sample, (H) heat-treated control sample, and (D) deformed sample.

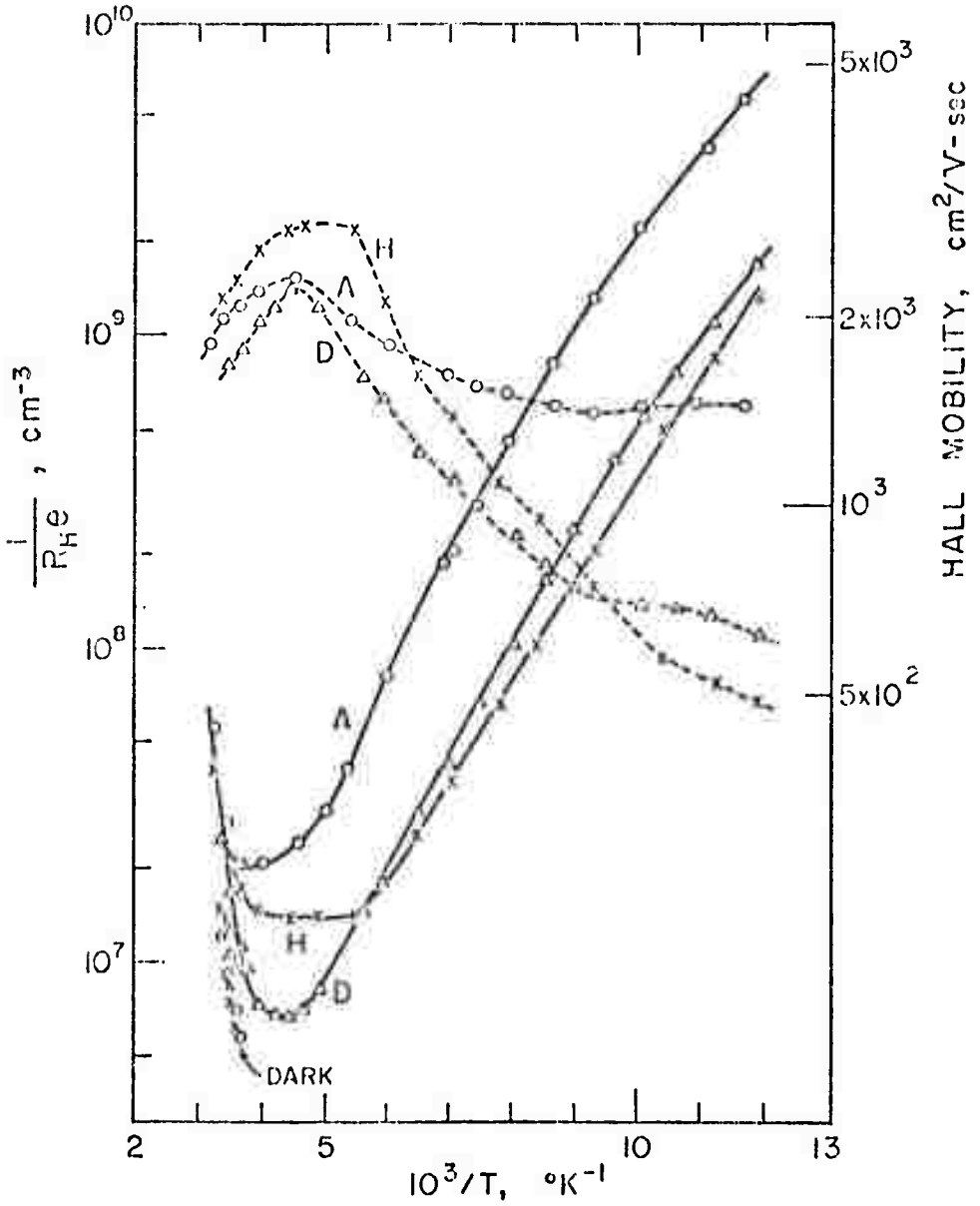

Figure V-11. Temperature dependence of the reciprocal Hall coefficient in the dark, and of the reciprocal Hall coefficient (solid curves) and of the Hall mobility (dashed curves) for extrinsic photoexcitation for the (A) as-grown sample, (H) heat-treated control sample, and (D) deformed sample.

VI. SCIENTIFIC ASPECTS OF SEMICONDUCTOR CRYSTAL PREPARATION

W. A. Tiller, B. Jindal and Hyo-Sup Kim

A. PROGRAM OBJECTIVES

The objective of this investigation is to develop an understanding of the important interfacial parameters that govern the growth of GaAs crystals. The study includes the structure and energetics of the GaAs solid/Ga-As liquid interface as a function of (i) the composition of the liquid phase and (ii) the orientation of the solid GaAs. In addition, the concentration distribution in the vicinity of the interface is to be calculated.

B. PROGRESS TO DATE AND PRESENT STATUS

The nature of the atomic interactions in the Ga-As system have been theoretically investigated and approximate interatomic potentials of the Morse type obtained by the parametric method. Later, more suitable potential functions for the GaAs crystal were determined by consideration of the individual binding mechanisms of atoms in the crystal. This information was utilized to obtain the quasi-chemical terms in the interfacial energy for planar perfect interfaces using the formal broken-bond method.

(1) More recently, the concentration distribution in the liquid at the interface region has been considered; it may be quite different from that of the bulk liquid solution due to the influence of interfacial fields. This problem has been solved employing the method of minimization of the total free energy of the system. In the calculation, the potential functions determined previously and the summation of planes method have been used. The free energy change associated with the phenomenon of redistribution can be written as

$$\Delta G = \Delta E + \Delta G_{chem} \tag{1}$$

where ΔE is the change of interphase interaction energy and ΔG_{chem} is the chemical free energy changes of the bulk which can be written as

$$\Delta G_{chem} = N_L \sum_p \sum_i \left\{ X_i^F \cdot \mu_i^F - X_i^I \cdot \mu_i^I \right\}_p \tag{2}$$

where X_i is the atomic fraction of component i; μ_i is the chemical potential of component i; N_L = area atomic density; the superscripts F and I refer to the final state, after concentration distribution changes, and the initial state, before concentration distribution changes, respectively; and the subscripts i and p refer to component i and the p^{th} atom plane respectively.

For the (100) GaAs/50 atomic % Ga-As melt, the concentration distribution at the interface was calculated and the results are given in Figure VI-1. The results show that there is Ga enrichment in the first layer of the liquid phase adjacent to the interface and depletion of Ga in the second and following layers with an asymptotic approach to the bulk concentration at about the 6th layer. In order to see the influence of the interchange energy of the liquid solution, the concentration distributions at the interface have been determined for the wide range of the interchange energy values from +6000 to -6000 cal/mole. In the absence of exact data on the activity coefficients in equation (2), it was assumed that the liquid could be characterized as a random regular solution with the activity coefficients, γ_i, given by

$$\gamma_i = \exp(X_i^2 \Omega / kT) \tag{3a}$$

and

$$\Omega = NZ \left[\varepsilon_{AB} - \frac{1}{2} (\varepsilon_{AA} + \varepsilon_{BB}) \right] \tag{3b}$$

where X_i is the atom fraction of i, Z is a coordination number and the ε_{ij} are interaction energies. To see the influence of Ω on the concentration distributions, Figure VI-1 considers the range of Ω from +6000 to -6000 cal/mole. For the larger values of Ω, the degree of enrichment of Ga at the interface increases. However, the same form of the distribution is retained for all values of Ω. For the Ga-As system, the value of Ω to be used should be close to -6000; however, an evaluation of the solution thermodynamics is needed in order to make this choice.

(2) The thermodynamic properties of the Ga-As liquid solution have been studied theoretically to explore the nature of the solution and to obtain useful data to use for determining atomic interaction energies and Ω in the liquid solutions. Proper concentration and temperature dependent functions of the activity coefficients have been obtained from which mixing quantities as a function of concentration and temperature have been determined. Figure VI-2 shows the heat, entropy and free energy of mixing vs. concentration at 1511°K. All the mixing quantities of this solution show very weak temperature dependence.

On the other hand, by generalizing the quasi-chemical approach including non-nearest neighbor interactions, short range order effects and the variation of bond energies with the mixing process, the energy of mixing as a function of bond energies has been derived as

$$E = Nx(1-x) \sum_{n=1} Z_n \left[\alpha_n \{\varepsilon_{AB,n} - 0.5\ (\varepsilon_{AA,n} + \varepsilon_{BB,n})\}\right.$$

$$\left. + 0.5\ \{(\varepsilon_{AA,n} - \varepsilon^{\circ}_{AA,n})/x + (\varepsilon_{BB,n} - \varepsilon^{\circ}_{BB,n})/(1-x)\}\right] \qquad (4)$$

where N is Avogadro's number, x is the atomic fraction of As atoms, Z_n is the coordination number of the n^{th} nearest neighbor, $\varepsilon_{ij,n}$ is the n^{th}

nearest neighbor interaction energy between atoms of component i and component j in the solution (i,j = A or B and A = Ga, B = As), $\varepsilon^{\circ}_{ii,n}$ is the n^{th} nearest neighbor interaction energy between atoms of component i in the pure state (i = A or B), and α_n is the short range order parameter of the n^{th} nearest neighbor expressed as

$$\alpha_n = 1 - x(1-x)\left(\frac{2\omega_n}{Z_n kT}\right) - \frac{1}{2}x(1-x)\{x-(1-x)^2\}^2\left(\frac{2\omega_n}{Z_n kT}\right)^2 + \ldots \qquad (5)$$

where ω_n is the interchange energy between n^{th} nearest neighbor and T is the temperature (°K) of interest. The first term in the bracket in equation (4) is the major contribution to the energy of mixing and the latter is due to the variation of the bond energies with mixing and is usually an order of magnitude smaller than the first. Using the data in Figure VI-2, the value of Ω is found to be -5485 cal/mole for the 50-50 solution at the liquidus temperature.

(3) Effective potential functions for pure liquid As and Ga have been determined by the parametric method using data on density, compressibility and atomization energy. The parameters of the potential functions of the Morse type are, for Ga,

$$\phi^{\circ} = 0.24921 \text{ (e.v.)}, \ \alpha = 0.98378 \ (A^{-1}), \ r^{\circ} = 3.40985 \text{ (A)} ,$$

for As,

$$\phi^{\circ} = 0.2006 \text{ (e.v.)}, \ \alpha = 0.80995 \ (A^{-1}), \ r^{\circ} = 3.62023 \text{ (A)} .$$

The interaction energies of the Ga-As liquid solution are considered as a mixed contribution of metallic, covalent, dispersion, and ionic interactions. The ionic interaction potentials due to partial ionization are similar to that found for other compound binary solutions and have been determined by calculating apparent charges of components by the Thomas-Fermi

approximation. Short-range order in the solution is primarily due to the ionic interaction. Effective potential functions of the Morse type for the other parts of the mixed contributions have been obtained by the parametric method, since further separation of the mixed contribution was not reasonable due to unavailability of information. The three parameters of the Morse potential function have been set as appropriate functions of concentration and temperature using fitting parameters; for the Ga-Ga or As-As interactions,

$$\phi^{\circ} = \phi^{\circ\circ}\left(1 + \frac{\Delta Z(X,T)}{Z}\right)^{n} \quad ; \quad r^{\circ} = r^{\circ\circ}\left(\frac{V(X,T)}{V^{\circ\circ}(T)}\right)^{1/3} \quad ;$$

$$\alpha = \alpha^{\circ\circ} + AX + BX^{2} + CX^{3} \quad , \tag{6}$$

where Z is the formal charge of the atom core ($Z_{AS} = 5$, $Z_{Ga} = 3$), ΔZ is the apparent charge of the atom core in the solution, V is the average volume of an atom, n, A, B, C, are the fitting parameters and the superscript $^{\circ\circ}$ refers to the pure state. For the Ga-As interactions, the Berthelot geometrical mean rule was applied. The best fitting parameters are $n = 0.0$, $\alpha_{Ga-Ga} = 0.98378 - 0.50071 \cdot X + 1.50736X^{2} - 1.23611X^{3}$, and $\alpha_{As-As} = 0.80995 + 0.30884 \cdot X - 0.30138X^{2} + 0.60281X^{3}$. Many other approaches have been explored to obtain more elegant potential functions but the attempts have not yet been successful. It does not seem fruitful to continue these attempts and we must be satisfied with the present level of modeling.

C. FUTURE WORK

Using the composition and orientation dependence of interface adsorption, the situation at layer edges will be evaluated to determine both interfacial energy and interface attachment kinetics as a function of

orientation and liquid composition. From the edge energy aspects, one can evaluate the ease or difficulty of creating layer edges at certain orientations. From the density of edge kinks and adsorbed Ga atoms, one can evaluate the driving forces needed for motion of the layer edges along faces of different orientations and along different directions in those faces.

In addition, using a recent theoretical advance relating to the creation of interfaces during phase transformations, the stability of different faceted interfaces in the GaAs system will be evaluated and a quantitative condition governing their breakdown developed. Using an experimental procedure involving the growth of bulk GaAs from solution at different temperatures and different supersaturations; this instability condition will be experimentally tested. The results of this experimental/theoretical correlation should be directly applicable to the epitaxial growth of GaAs layers.

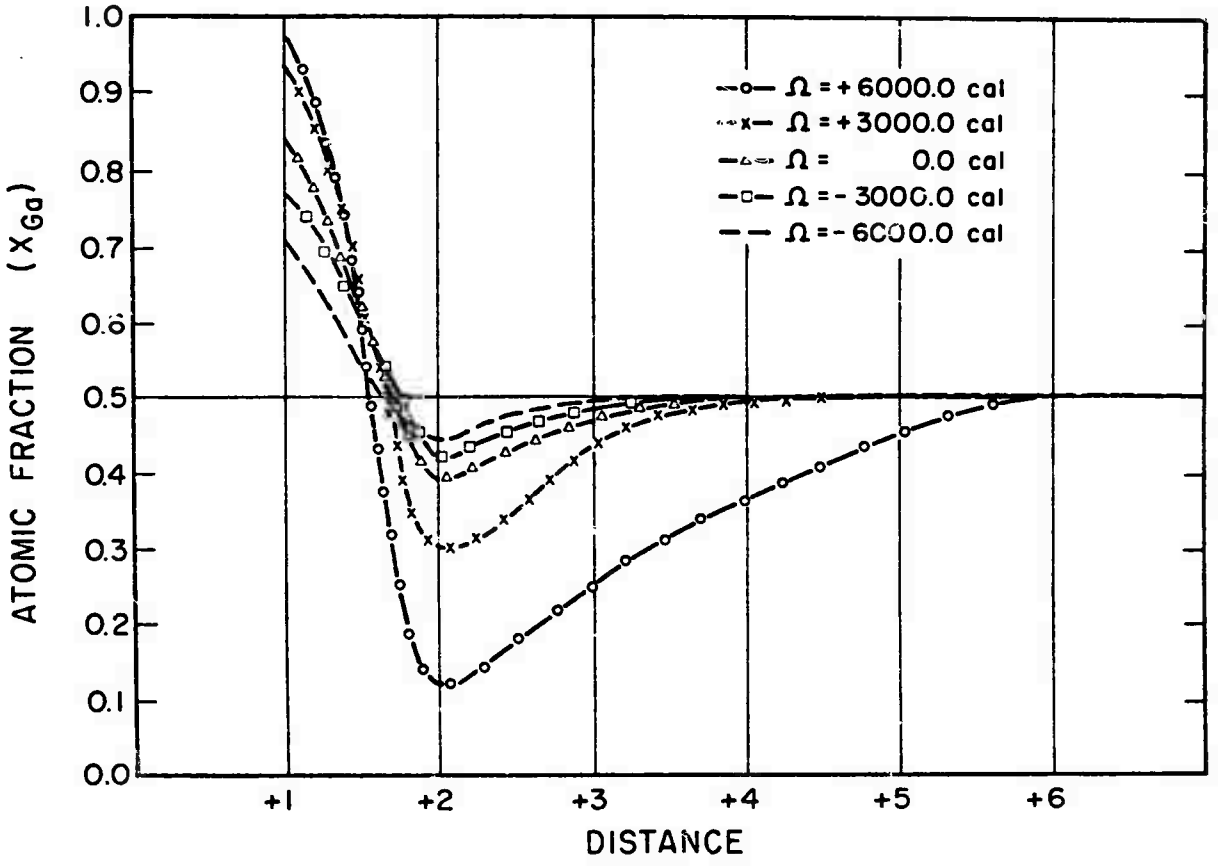

Fig. VI-1. Concentration distributions in the Ga-As melt ahead of a (100) interface of GaAs (A-face).

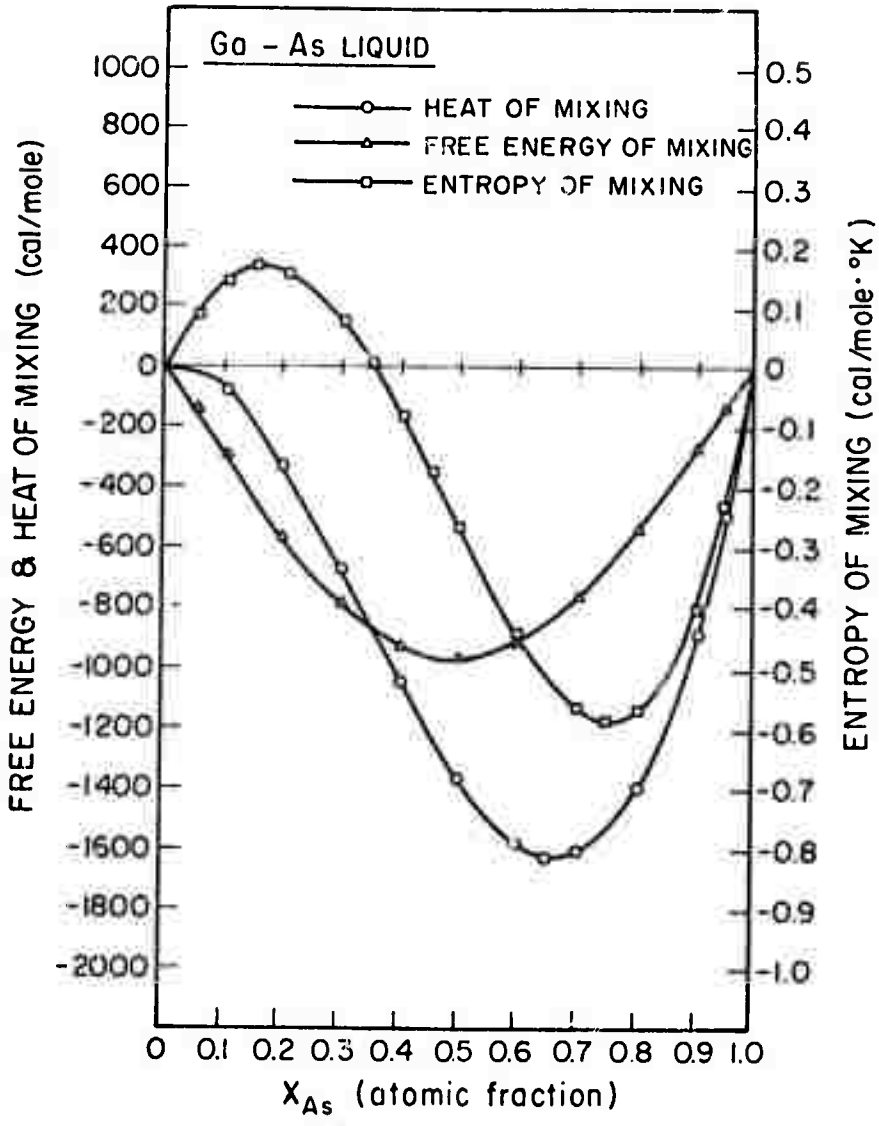

Fig. VI-2. Thermodynamic properties of Ga-As liquid at 1511°K.